MASTER'S DEGREE THESIS

MSc in Applied Mathematics

Title: Impact sound insulation using SEA

Author: Marcel Janer

Advisors: Jordi Poblet-Puig , Antonio Rodriguez-Ferran

Department: Matemàtica Aplicada III (727)

Academic year: 2009-2010

Facultat de Matemàtiques i Estadística

UNIVERSITAT POLITÈCNICA DE CATALUNYA

Contents

Acknowledgements

I would like to thank Antonio Rodriguez-Ferran, Jordi Poblet-Puig and Cristina Díaz Cerceda for helping me in the development of this Master Thesis and for all their ideas and comments related to my problems with the simulations. This work would not have been possible without them.

I would like to thank Oriol Guasch and Pere Artís for their advises and their unconditional support.

I also would like to thank Ferran Bermejo for giving me the possibility of having the necessary tools to make this research and also all my workmates from iMat for creating such a friendly atmosphere.

Finally I would like to thank all my friends and my family, who make it all worthwhile.

Nomenclature

α	Mean absorption coefficient
Δf	Frequency bandwith
ΔL	Impact sound reduction due to floor coverings
η_{ij}	Coupling loss factor between subsystem i and subsystem j
η_i	Damping Loss Factor of subsystem i
ρ	Density of the air
σ	Radiation efficiency
τ_{ij}	Structural transmission coefficient between elements i and j
ξ	Mean free path for a diffuse field in a plate
A	Equivalent absorption area of the cavity
$a_{i,situ}$	Equivalent absorption length of the element i
c	Velocity of sound in air
c_e	Velocity of sound in an elastic medium
c_g	Group velocity for the energy in a plate
E	Energy of a subsystem
f_c	Critical frequency of a floor
f_d	Frequency for standing waves in an elastic medium
f_{f0}	Frequency of resonance of a floating floor
F_{rms}	Mean squared force of the tapping machine
f_{s0}	Resonance frequency of a soft floor covering
k_d	Dynamic stiffness of an elastic material
K_{ij}	Vibrational reduction index between elements i and j

L	Impact sound pressure level
L_n	Normalised impact sound pressure level
L_{cav}	Sum of the length of all edges of the cavity
$L_{n,d}$	Normalised impact sound pressure level for the direct path
$L_{n,ij}$	Normalised impact sound pressure level due to the flanking path through subsystems ij
$L_{n,W}$	Weighted normalised impact sound pressure level
M_h	Mass of the ISO tapping machine hammer
m_s	Surface density of a plate
n_i	Modal density of the subsystem i
p	Averaged pressure
p_0	Reference pressure ($2 \cdot 10^{-5} Pa$)
P_i	External input power in a subsystem i
$P_{i,dis}$	Power dissipated in a subsystem i
P_{ij}	Power flowing from subsystem i to subsystem j
R	Sound reduction index
R_{situ}	Sound reduction index for in situ conditions
S_h	Area of impact of the ISO tapping machine hammer
S_i	Area of the plate subsystem i
S_{cav}	Surface of the cavity
T_{lab}	Structural reverberation time in laboratory
T_{situ}	Structural reverberation time *in situ*
V_{cav}	Volume of the cavity
w	Frequency in radians
Y	Plate mobility

Introduction

This master thesis deals with the application of a particular modeling technique in predicting the impact sound insulation of a floor. The method analyzed is the Statistical Energy Analysis (SEA), developed in 1960 to solve vibroacoustic problems related to the aerospace industry. In particular, we want to study the capacity of SEA to properly simulate the behavior of different building solutions to impact noise. In most of the parts of this work, a SEA commercial software (VA-One) has been used because I have acces to it in my place of work (iMat - Construction Technological Center). Thus, we have also evaluated the versatility of the program to model these building solutions.

Referring to the predictions made, chapters 3 and 4 deal with direct transmision while chapters 5 and 6 study the transmission of sound through the flanking elements. Besides, in chapters 3 and 5 the results obtained with SEA are compared with the results obtained with a modal approach. Finally, throughout the paper, most of the results are compared with experimental data obtained from different articles in order to validate the simulations.

The outline of this work is as follows:

In the first chapter we present a brief state of the art of the impact sound prediction methods and the current regulatory requirements.

In the second chapter we give a brief overview of the SEA method.

In the third chapter we make an analysis of the impact sound insulation on a single plate. The results of this analysis are compared with experimental data and with a numerical simulation realized using a modal approach. In this part we have also compared the solution of the commercial software with our own SEA code. Finally, a parametric analysis has been done with the goal to determine the sensitivity of the impact sound pressure level to the properties of the floor.

In the fourth chapter we have evaluated VA-One's ability to simulate the behavior of resilient coverings and floating floors to the impact sound insulation.

In the fifth chapter we have analyzed the transmission of the impact noise through different plates. In this case, the influence of the stiffness of the junction between the plates as well as the influence of the thickness of the plates are studied. The results are compared with the modal approach.

In the sixth chapter we have studied the importance of flanking transmission in the impact sound insulation between two dwellings. In this case we have shown the benefits from using SEA instead of the methodology of the European regulation.

Finally we present our conclusions and some future work that can be done.

Chapter 1

State of the art

1.1 Legal sound insulation requirements

Last year, the new Spanish Building Regulation (CTE DB - HR) came into force replacing the standard NBE - CA88. According to this old standard, the acoustical performance of a building was characterized by means of the laboratory sound insulation measurement for each element composing the building. The new regulation has increased the legal sound insulation requirements and has considered the whole building as a product itself in order to guarantee the acoustical quality of dwellings. Among them, one of the regulatory requirements that has been increased is the impact sound insulation. The new DB - HR establishes a maximum permissible value for the weighted standardized impact sound pressure level of $L'_{nT,w} \leq 65$ dB [DB-HR, 2007]. This single-number magnitude is described in the ISO 717 - 2 [ISO, d] and, to predict this magnitude based on laboratory testing of building materials, the standard UNE EN ISO 12354 Part 2 should be followed [ISO, b].
In the calculation of both the insulation from airborne noise and the insulation from impact noise, we need to know the input and output sound power. When we are dealing with airborne noise, the acoustical requirement is a ratio of both sound powers and a minimum number has to be achieved. However, in impact sound insulation, a normalized source has been defined and the acoustical requirement refers to the quantity of output sound power allowed, so a maximum value is defined in the regulation.

1.2 ISO tapping machine

Measuring the input sound power in a floor to determine the impact sound insulation is a complex issue due to the very different nature of impact sources and the relation between the input force and the kind of floor that we are trying to characterize. To solve this drawback a standardized source has been defined in the ISO 140-6, the *normalized tapping machine* [ISO, c].
In the tapping machine there are five hammers weighting 500 grams, aligned and equally spaced 100 mm and falling from a height of 40 millimeters to hit the floor 10 times per second. Detailed specifications about the geometry of the hammers are given in the standards and accurate specifications are needed because small changes

in the design affect the input power in the system substantially.
For years, the ISO tapping machine has been criticized in relation with its incapacity to represent a particular type of impact, like footsteps or a child jumping. Other problems found are the effect of the hammer impedance in the floor and the non linear response of some soft floor coverings [Hopkins, 2007]. The same criticisms about its correlation with subjective perceptions of sound insulation apply to the rating system used to produce a single-number quantity.
Alternative impact machines, as the bang machine or the rubber ball, have been proposed to simulate heavy soft impacts and are included in the Japanese Standard JIS A 1418-2. These machines are thought to be better suited for predicting the sound insulation of lightweight floors. However, the level measured cannot be normalised to the absorption area or standardized to the reverberation time of the receiving room so it is difficult to compare results from different measurements. Related to the classification method, different weighted coefficients have been proposed, by Bodlund with emphasis on the low-frequency range [Bodlund, 1985]. Although its rating system is not directly implemented in the regulations, there is a coefficient that has taken into account low frequency terms ($C_{l,50-2500}$). In any case, this coefficient is hardly ever used in the regulatory requirements [Rasmussen, 2009] so we will not use it in this work.

1.2.1 Modeling the tapping machine

In order to be able to predict the impact sound insulation performance of a floor we need to know the force spectrum created by the tapping machine. The spectrum obtained will depend on the kind of floor considered and the simplifications made in the model. The simplest model and one of the most common is the constant force spectral density formulated by Vér that gives a mean squared force of [Vér, 1971]

$$F_{rms} = \sqrt{4\Delta f}, \tag{1.1}$$

where Δf is the effective bandwith of the frequency band considered (in our approach, we will use third-octave bands because they give more information than octave bands).This model assumes short duration impacts and only takes into account the impedance of the hammer.
A more complete model that includes the effect of the contact stiffness and the floor impedance on the force applied by the hammer is the so called *lumped element model* developed by Lindblad [Lindblad, 1968] and used by Brunskog and Hammer in [Brunskog and Hammer, 2003]. In this Master Thesis, the lumped element model will be used.

1.3 Prediction methods

To meet impact sound insulation requirements, appropiate prediction tools are important. These tools can be classified into two groups: deterministic methods and statistical methods. Moreover, as explained in section 1.1, the new regulation is concerned with the whole building acoustical behavior, so when predicting the impact sound insulation we have to take into account not only the *direct transmission* across the separating floor but also the *flanking transmission* via adjacent building elements.

In the prediction of direct impact sound insulation, there are few analytical deterministic methods in the literature. The methods most used are simple relationships, like the one proposed by Vér between the transmission loss and the normalised impact sound pressure [Vér, 1971] or the equations based on the work of Gerretsen for homogeneous floors included in the Annex B of reference [ISO, b]. In the field of numerical methods, deterministic numerical models based on modal analysis have been developed recently to address the direct impact sound insulation problem with good results [Díaz, 2009],[Hetherington, 2009]. Also, some expressions based on Statistical Energy Analysis have been derived to deal with the direct transmission of impact sound (see page 510 in [Hopkins, 2007] or the work done in [Stewart and Craik, 2000]).

In the prediction of flanking transmission, Statistical Energy Analysis has been considered as the most suitable method and, in fact, the method used in the standards UNE EN ISO 12354 parts 1 and 2 has been shown to be the same as the SEA method when only first-order flanking paths are considered [Nightingale and Bosmans, 2003].

Chapter 2

Statistical Energy Analysis

Statistical Energy Analysis (SEA) is a probabilistic method to predict the vibration and sound transmission in dynamic and complex systems. This method studies the energy exchange between groups of modes when conservation of energy is imposed. Due to its collective behaviour, SEA can be described as the thermodynamics of structural and acoustical vibrations [Le Bot and Cotoni, 2009].

2.1 History and Development

The method arose in 1959 with two independent related works from Lyon and Smith about the radiation properties of resonators. With the collaboration of Maidanik, the first articles about SEA appeared in 1960 and showed the main relevant parameters when predicting the acoustical behavior of a system [Lyon, 1975]. Since then, two independent lines of research were established : the knowledge of the basic requirements to implement the method and the extension of the theory to more realistic models.
The initial success of SEA in the prediction of the vibroacoustic behavior took place in the aerospace industry and, from there, its use became widespread in sectors such as automotive and railway industries, where the vibrations at high frequencies were important. The beginnings of using the SEA method for building acoustics is found in [Price and Crocker, 1970]. Even so, being a less technological sector has meant that its use is not as widespread as in other fields. A summary of all the capabilities of the method in building acoustics, along with many examples of predictions can be found in Craik's book [Craik, 1996].
In the other line of research, study of the conditions is primarily the study of confidence intervals of the SEA. As a probabilistic approach, it is fundamental to know the uncertainty of the results. 'While the study of the influence of the *modal overlap factor* or the *modes per band* is not clear, the SEA method will be fully reliable only in the region of high frequencies, where the conditions for statistical analysis are satisfied'[Fahy, 1994]. Although there are still no formal procedures to obtain the level of uncertainty, some progress has been made recently (see [R.S Langley, 2004] and [Brown, 2003]). In any case, in this work, only the extension of the method to building models will be studied while the error analysis is postponed for further work.

2.2 Basics

Statistical Energy Analysis provides an estimate of the equilibrium energies in a network of *subsystems* that are subjected to a distribution of stationary external forces over time.
The subsystem is an abstract concept and it does not need to be represented by a physical entity. In particular, one might define a subsystem as a group of modes of vibration. Thus, a plate containing one flexural wave and two longitudinal waves must be modeled as three subsystems. Although there are no specific rules to make a selection of subsystems, there are some clear guidelines to be considered [ESDU, 1999]:

- For each frequency band, each subsystem must contain a minimum of modes with the fundamental frequency within the band.
- There must be equipartition of vibrational energy between modes. This means that each mode should contribute more or less the same to the overall energy of the subsystem.
- Ideally, subsystems must be weakly coupled. This means that if a subsystem is subject to an excitation, the response of this subsystem must be greater than the response of any other subsystem.

The degrees of freedom in SEA are the vibrational energies of the subsystems. The vibrational energy is the sum of the kinetic and potential (strain) energies associated with the motion of the subsystem. The rate of energy exchange between subsystems corresponds to power transmission and the rate of energy dissipation from a subsystem corresponds to dissipated power. On the one hand, the power transfer between two subsystems i and j is governed by the *Coupling Loss Factor* η_{ij}, that depends upon the properties of the subsystems and the way in which the subsystems are coupled. On the other hand, the dissipation of power in a subsystem i is governed by a parameter called the *Damping Loss Factor* η_i. Finally, the estimation of the energy levels leads to a set of power balance equations.

SEA expressions are based in the modal-wave duality and it is common to derive the SEA parameters by modal analysis or by wave propagation in a semi-infinite medium. In this master thesis we will use the modal view to build the power balance equations and to define all the SEA parameters except the coupling loss factors between two plates, which will be defined using the wave approach.

Chapter 3

Analysis of impact sound on a single plate

3.1 Predicting the impact sound insulation in a real case

In order to be able to evaluate the performance of SEA when modeling impact sound insulation, we use an experimental measurement done by Ford and Warnock and documented in [Ford et al., 1974]. The floor studied is a slab of bare concrete whose properties are presented in table 3.1.

Meaning	Value
Density	2400 Kg/m^3
Young modulus	30 GPa
Poisson's ratio	0.2 GPa
Lateral dimensions	2.4 m $\times$ 2.4 m
Thickness	0.1 m

Table 3.1: Concrete slab properties

The analysis is realized in third octave bands and the lumped model from section 1.2.1 is used to obtain the tapping machine's force spectrum. The damping loss factor is obtained interpolating the values given in octave bands in reference [Ford et al., 1974].

f (Hz)	31.5	40	50	63	80	100	125	160	200	250	315
η	0.05	0.052	0.053	0.055	0.049	0.044	0.04	0.031	0.025	0.02	0.018
f (Hz)	400	500	630	800	1000	1250	1600	2000	2500	3150	4000
η	0.0166	0.015	0.012	0.0098	0.008	0.008	0.008	0.008	0.0073	0.0066	0.006

Table 3.2: Loss factor

The simulation in SEA is realized using the commercial software VA-One. In figure 3.1 we find a picture of the simple model used. We obtain as an output the

sound pressure level of the cavity and, from this we find the *normalised impact sound pressure level* by

$$L_n = L + 10 \log \frac{A}{10}. \tag{3.1}$$

Where A is the equivalent absorption area of the cavity (which is equal to the mean absorption α times the cavity's surface S_{cav}). In this case, the dimensions of the cavity are 2.4 × 2.4 × 2 and the mean absorption used is the 18 %. In figure 3.2

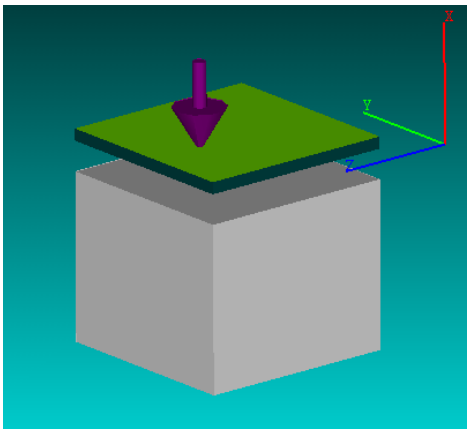

Figure 3.1: VA-One model

we can see the results obtained in comparison with the experimental ones and with the two simulations realized in the modal approach with and without considering the finite size of the plate [Díaz, 2009]. From the graph , we can state that the prediction

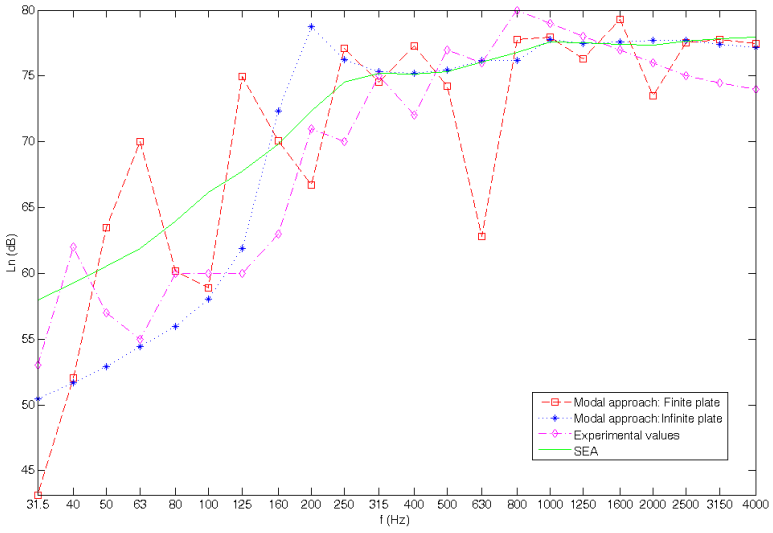

Figure 3.2: Normalised impact sound pressure level

at high frequencies with SEA is almost the same as the values obtained with the modal approach. On the other hand, the values obtained at low frequencies with SEA underestimate the impact sound insulation.

3.2 Building the SEA matrix

In this section, a simple model related to the direct impact sound transmission is going to be developed. The aim is to show the simplicity of the equations governing the SEA method when few subsystems are considered. In subsection 3.2.1 power balance equations are developed, in subsections 3.2.2, 3.2.3, 3.2.4, 3.2.5 and 3.2.6 there is a detailed explanation of all the parameters used in the model. Finally, in subsection 3.2.7 we compare the solution obtained with the one given by the commercial software VA-One.
All the following analysis is done considering that we only have bending modes in the floor.

3.2.1 Power balance equations

In a general form, the power balance equations for a subsystem i are

$$P_i + \sum_{j=1, j\neq i}^{N} P_{ji} = P_{i,dis} + \sum_{j=1, j\neq i}^{N} P_{ij}. \tag{3.2}$$

Where P_i is the external input power in the subsystem i, P_{ji} is the power received in the subsystem i from a subsystem j, P_{ji} is the power transmitted from the subsystem i to a subsystem j and $P_{i,dis}$ is the power lost in the subsystem i due to dissipation. Now we introduce the coupling loss factors (CLF), defined as *the fraction of energy transmitted from one subsystem to another in one radian cycle*, so the power flow between two subsystems i and j is

$$P_{ij} = E_i w \eta_{ij}, \tag{3.3}$$

where E_i is the energy of the subsystem i and w is the angular frequency. In a similar way, the damping loss factor (DLF) is defined as *the fraction of energy lost from subsystem i as heat or as energy transmitted to other parts of the structure not included in the model* and the fraction of energy lost in a subsystem is [Craik, 1996]

$$P_{i,dis} = E_i w \eta_{i,dis}. \tag{3.4}$$

Substituting these expressions in the power balance equations we obtain

$$P_i = w\eta_i E_i + \sum_{j=1, j=\neq i}^{N} w\eta_{ij} n_i \left(\frac{E_i}{n_i} - \frac{E_j}{n_j} \right), \tag{3.5}$$

where we have introduced the modal densities (n_i and n_j). Even if we use the expressions without these parameters, modal densities are indispensable to get the coupling loss factors and the input power (see subsections 3.2.4 and 3.2.6).
In our specific case, if we only consider bending waves and neglect the influence of other kinds of waves, the overall system is composed of only two groups of modes (two subsystems). On the one hand, we have a structural subsystem modeling an homogeneous floor and, on the other hand, an acoustic subsystem that corresponds

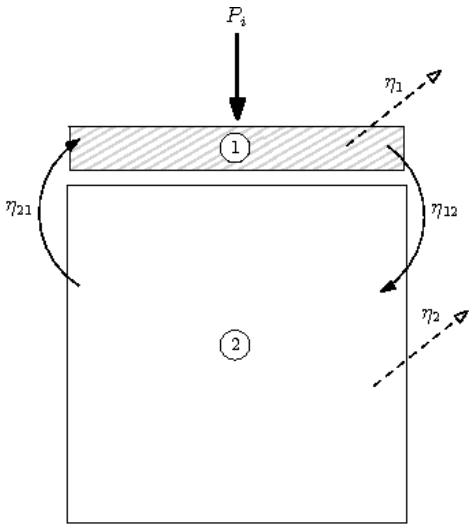

Figure 3.3: Model considered

to a room. As we can see in figure 3.3, the external power input (tapping machine) is connected to the structural subsystem. In this section, subindex *1* is related to the structural subsystem and subindex *2* refers to the acoustical subsystem.

Thus, writing the power balance equations for our subsystems, we get

$$P_i = w\eta_1 E_1 + w\eta_{12} n_1 \left(\frac{E_1}{n_1} - \frac{E_2}{n_2} \right) \tag{3.6}$$

$$0 = w\eta_2 E_2 + w\eta_{21} n_2 \left(\frac{E_2}{n_2} - \frac{E_1}{n_1} \right), \tag{3.7}$$

and, rewriting the equations in a matrix form we obtain

$$w \begin{bmatrix} \eta_1 n_1 + \eta_{12} n_1 & -\eta_{12} n_1 \\ -\eta_{21} n_2 & \eta_2 n_2 + \eta_{21} n_2 \end{bmatrix} \begin{pmatrix} \frac{E_1}{n_1} \\ \frac{E_2}{n_2} \end{pmatrix} = \begin{pmatrix} P_i \\ 0 \end{pmatrix}. \tag{3.8}$$

This matrix is symmetric due to the consistency relationship (3.20). Operating with the modal densities, we can write it in a nonsymmetric form as

$$w \begin{bmatrix} \eta_1 + \eta_{12} & -\eta_{21} \\ -\eta_{12} & \eta_2 + \eta_{21} \end{bmatrix} \begin{pmatrix} E_1 \\ E_2 \end{pmatrix} = \begin{pmatrix} P_i \\ 0 \end{pmatrix}. \tag{3.9}$$

Finally, solving the system we obtain

$$E_1 = \frac{(\eta_2 + \eta_{21})\, P_i}{w\left(\eta_1\eta_2 + \eta_1\eta_{21} + \eta_2\eta_{21}\right)} \tag{3.10}$$

$$E_2 = \frac{P_i}{w\left(\frac{\eta_1}{\eta_{12}}\left(\eta_2 + \eta_{21}\right) + \eta_2\right)} \tag{3.11}$$

We can see that with a very simple set of equations, our system is fully described with SEA and the only difficulty is to find the analytical expressions for all the SEA parameters needed.

3.2.2 Modal densities

Modes or resonances occur when there is a steady state wave that forces the subsystem to oscillate in phase. Statistical Energy Analysis assumes that the response of the subsystem is due to these resonances and that any other motion can be ignored [Craik, 1996]. This means that the number of modes of a subsystem is an important variable to consider when modeling in SEA. Equivalently, we define the modal density as the number of modes that lie in an increment of frequency of 1 rad/s.

$$n(w) = \frac{dN}{dw} \tag{3.12}$$

For some simple elements, there are analytical expressions for the modal density in the literature. In the case of the floor, if we assume that our subsystem behaves as a simply supported plate and we only consider bending waves, the modal density is given by[1] [Cremer et al., 2005]

$$n_1(w) = \frac{S f_c}{2c^2}, \tag{3.13}$$

where f_c is the critical frequency of the floor. In the case of a cavity, the analytical expression for the modal density is [Arau, 1999]

$$n_2(w) = \frac{2f^2 V_{cav}}{c_0^3} + \frac{f S_{cav}}{4c_0^2} + \frac{L_{cav}}{16\pi c}. \tag{3.14}$$

3.2.3 Damping loss factor

The general name for the mechanisms that cause energy to be lost is damping. In building acoustics, a common measure of damping is the reverberation time in cavities and structural reverberation time in solids (T). In SEA, the measure of damping that is used is the damping loss factor η, which is related to the structural reverberation time by

$$\eta = \frac{2.2}{fT}. \tag{3.15}$$

The damping loss factor (DLF) is defined as the fraction of energy lost in one radian cycle and both empirical data and analytical expressions are available to estimate its value. In our work, an empirical DLF for the floor is given, so we will use the values of table 3.2. In contrast, the damping loss factor for the cavity will be obtained from its absorption coefficient α using the following expression [Craik, 1996]

$$\eta_2 = \frac{c\alpha S_{cav}}{8\pi f V_{cav}}. \tag{3.16}$$

The absorption coefficient used in our model is $\alpha = 0.18$. In any case, as our output is the normalised impact sound pressure, its contribution is subtracted using (3.1) and its influence in the results is minimum.

[1] Although it has no explicit dependence on w, we write n(w) to emphasize that we are working with radians.

3.2.4 Coupling Loss Factors

Coupling loss factors (CLF) are the parameters that describe the sound transmission from one subsystem to another. SEA is the only method that uses these parameters and, except for some simple models, they are difficult to obtain. In our model we have only two coupling loss factors that take into account the vibration transmission from the floor to the cavity and vice versa.
To calculate these CLFs, we start writing down the power radiated by a wall of area S vibrating with a velocity v [Craik, 1996]

$$P_{12} = v^2 \rho c S \sigma, \tag{3.17}$$

where σ is the radiation efficiency and will be analyzed in the next section.
On the other hand, by definition of the CLF (3.3) and assuming that the vibrational energy of a plate is $E_1 = Mv^2$, where M is its total mass , the power transmitted between these subsystems is

$$P_{12} = m_s S v^2 w \eta_{12}. \tag{3.18}$$

Equating both expressions, the coupling loss factor for the radiation from a plate to a cavity is

$$\eta_{12} = \frac{\rho c \sigma}{2\pi f m_s}. \tag{3.19}$$

Finally, to find the coupling loss factor that governs the transmission from the cavity to the plate we can use the *consistency relationship*

$$n_1 \eta_{12} = n_2 \eta_{21}. \tag{3.20}$$

This relationship allows us to calculate η_{21} once we know the modal densities of each subsystem.

3.2.5 Radiation efficiency

We have seen that the coupling between a plate and a cavity is related to the radiation efficiency of the plate. The radiation efficiency is defined as "the power radiated by an object in comparison with the power radiated by a piston of the same area" [Cremer et al., 2005]. In the literature we can find several analytical expressions to estimate the radiation efficiency of a simply supported rectangular plate. In this work, we use some of these expressions to compare their results with the radiation efficiency given by the VA-One.
On the one hand, we obtain the radiation efficiency using the classical formulation given by Maidanik with the correction made by Renji at low frequencies [Renji et al., 1998]. On the other hand, we also compute the radiation efficiency obtained by Leppington [Leppington and Broadbent, 2002] because it is the method on which the VA-One is based [ESI-GROUP, 2009]. Finally, we plot the radiation efficiency obtained using the expressions given in the annex B of UNE EN 12354-1 [ISO, a]. These expressions are based on the work of Maidanik for high frequencies, whereas at low frequencies

the transmission due to forced waves is introduced using the formulation of Sewell [Sewell, 1970].

Looking at figure 3.4 we see that we have differences around the critical frequency (the frequency at which the radiation of the plate is maximum). In the case of a square flat plate of 2.4 meters (figure 3.4a) VA-One results seem to mistake the critical frequency and both Leppington and Maidanik results have sharp transitions between low and high frequency predictions. On the other hand, in the case of a square flat plate of 8 meters (figure 3.4b) all the methods give similar results and estimate the critical frequency correctly.

In this work, VA-One results will be used in order to be able to compare our own code with the VA-One solution although the radiation given in the ISO annex seems to display the best behaviour of all.

For deeper analysis, different expressions for the forced radiation can be found in [Davy, 2009] while different corrections to estimate the efficiency of radiation are presented in [Hopkins, 2007].

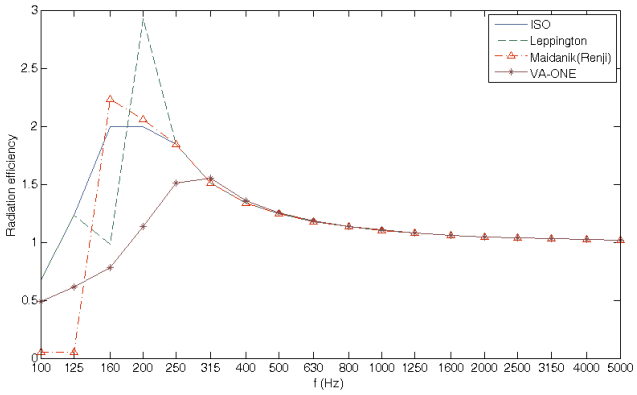

(a) 2.4 m x 2.4 m flat plate

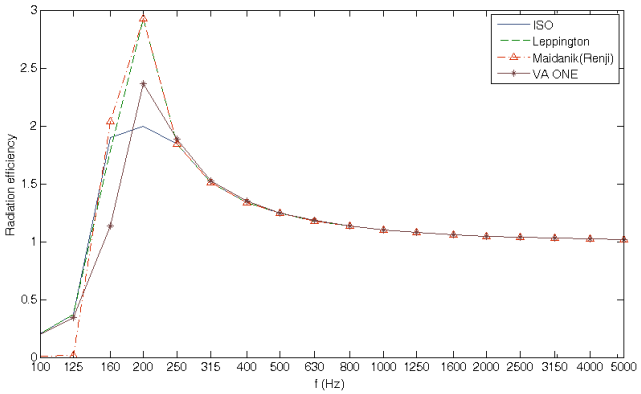

(b) 8 m x 8 m flat plate

Figure 3.4: Analytical expressions of the radiation efficiency of a simply supported plate

3.2.6 Input power

In order to solve our SEA system of equations, we need to introduce an input power that represents the power made by the impact of the hammers of the tapping machine. As we can consider that the source is a point force, the input power is given by [Craik, 1996]

$$W = F_{rms}^2 \Re(Y). \tag{3.21}$$

In our case, the force spectra F_{rms} is obtained using the lumped element model presented in [Brunskog and Hammer, 2003] while the real part of the mobility for a point-excitation of a plate is given by [Cremer et al., 2005]

$$\Re(Y) = \frac{\pi n(w)}{2Sm_s}. \tag{3.22}$$

3.2.7 Solving the system

At this point, we have identified all the necessary parameters required by SEA, so we can solve the matrix to obtain the energies in both subsystems. Then, the relationship between the average pressure and the energy in the cavity is given by

$$p^2 = \rho c^2 \frac{E_2}{V_{cav}}. \tag{3.23}$$

And the *normalised impact sound pressure level* is

$$L_n = 20 \log \frac{p}{p_0} + 10 \log \frac{A}{10}. \tag{3.24}$$

In figure 3.5 we compare the results with the solution obtained by means of the commercial software VA-One and we find that they are almost identical.

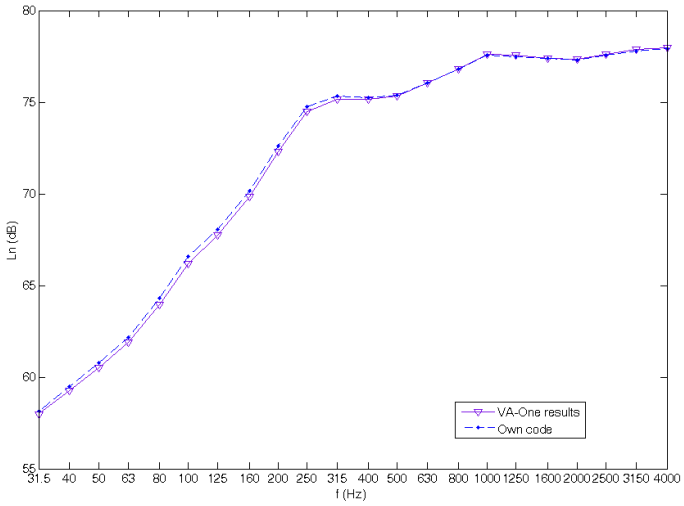

Figure 3.5: Normalised impact sound pressure level

3.3 Parametric analysis

In this section we perform a parametric analysis to determine which properties are more relevant for the impact sound insulation of an homogeneous concrete floor. Taking as reference floor the one analyzed previously, we change the values of its main properties to evaluate the sensitivity of the sound pressure level in the receiving cavity. Without diminishing the scope of the work, a constant loss factor in all frequency bands is considered in order to make the analysis of this parameter easier. The value chosen is the one corresponding to a value of 500 Hz, $\eta = 0.015$.

The normalised impact sound pressure levels obtained are plotted in figures 3.6 and 3.7.

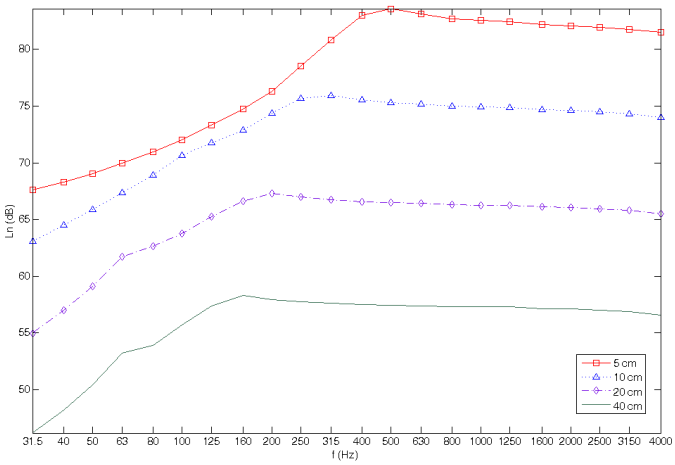

(a) Thickness

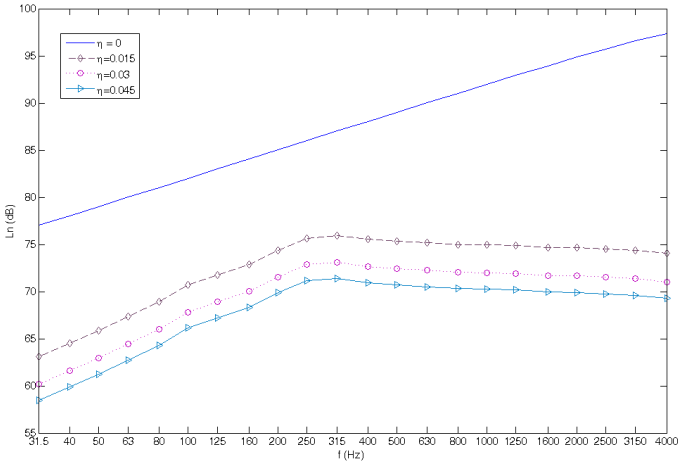

(b) Loss Factor

Figure 3.6: Normalised impact sound pressure levels

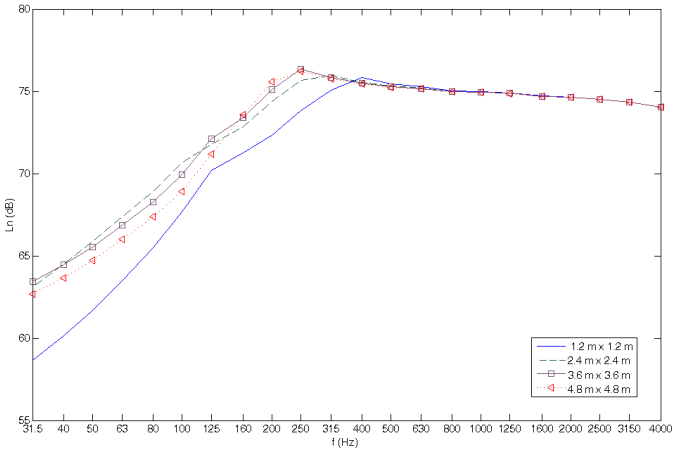

(a) Dimensions

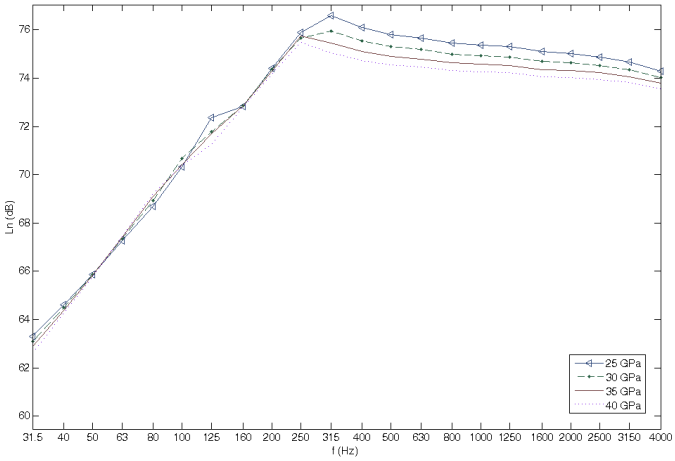

(b) Young Modulus

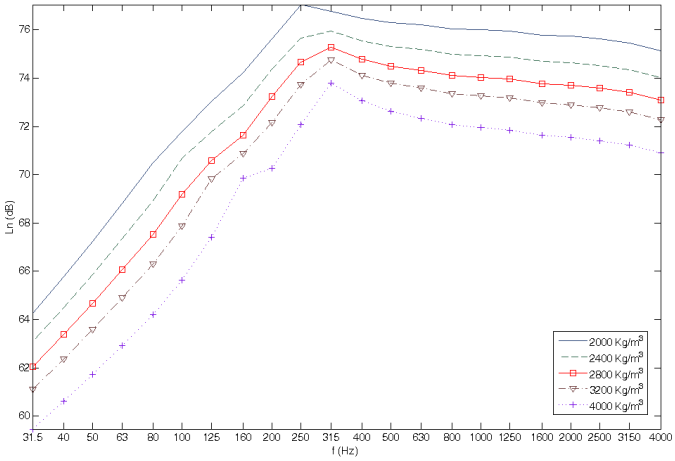

(c) Density

Figure 3.7: Normalised impact sound pressure levels

Looking at the graphs we observe that, on the one hand, the variation of the sound pressure levels takes place in the whole frequency range when we change the thickness, the loss factor or the density. On the other hand, increasing the Young Modulus only affects the range above 300 Hz while changing the lateral dimensions of the floor only produces variations in the sound pressure level below 400 Hz.
Finally, we can also see that when we have a null loss factor we obtain a very high sound pressure level linearly related to the logarithm of the frequency. As the SEA is a method where all the transmission is considered damping-controlled, it is obvious that without damping, the transmission will be very high. The shape of the curve can be understood setting $\eta_1 = 0$ in (3.11) and assuming that the input force is constant. Then, using (3.16) we can see that there is a lineal relationship between the energy of the cavity and the frequency so $L \propto \log E \propto \log f$.

In table 3.3 we see the values obtained for the *weighted normalised impact sound pressure level* $L_{n,W}$ in each simulation. The calculation of this weighted magnitude has been done as described in [ISO, d].
Looking at the results, we can observe that doubling the thickness of the floor the impact sound insulation increases by **9 db**, doubling the density the impact sound insulation increases by **4 dB** and, if we double the loss factor, the impact sound insulation increases by **2-3 dB**. The Young Modulus and the lateral dimensions have almost no effect on the weighted value.
Although in real materials these properties are linked and their influence cannot be isolated, this analysis highlights the importance of some parameters like the damping loss factor and allows a quantitative evaluation of the behavior of a concrete floor knowing its geometric properties.

Thickness (cm)	$L_{n,W}$ (dB)
5	88
10	81
20	72
40	63

Loss Factor	$L_{n,W}$ (dB)
0	101
0.015	81
0.03	78
0.045	76

Lateral dimensions (m)	$L_{n,W}$ (dB)
1.2 x 1.2	81
2.4 x 2.4	81
3.6 x 3.6	81
4.8 x 4.8	81

Young Modulus (GPa)	$L_{n,W}$ (dB)
25	81
30	81
35	80
40	80

Density (Kg/m^3)	$L_{n,W}$ (dB)
2000	82
2400	81
2800	80
3200	79
4000	78

Table 3.3: Weighted normalised impact sound pressure level values

3.3.1 Comparison with the modal approach

The results of the parametric analysis are compared with those obtained in reference [Díaz, 2009] by means of modal analysis. In figure 3.8 we see that both methods have given very similar values. Moreover, the SEA method almost always give an impact sound pressure level equal or 1 dB higger than the numerical methods. Thus, we can consider that the results are quite satisfactory.

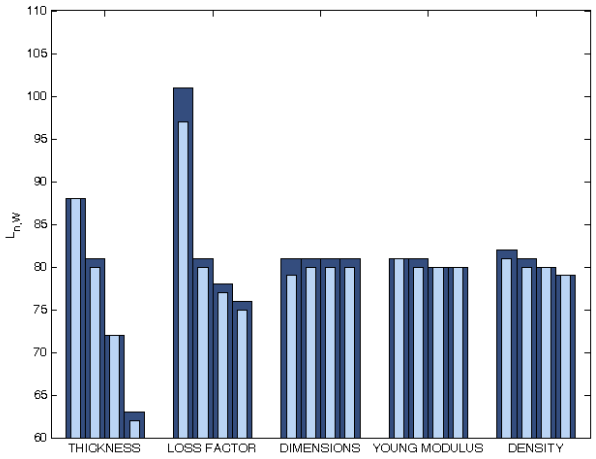

Figure 3.8: Comparing SEA results (dark blue) with numerical methods results (light blue). The previous analysis is summarized here and all the parameters are ordered from lower to higher values

Chapter 4

Predicting the reduction of impact noise due to floor coverings

As we have seen in section 3.3, the thickness of the slab is the parameter that has most influence in impact sound insulation. If a floor is close to meeting the requirements, increasing the thickness may be a solution. Whereas, if we have to reduce the impact sound pressure level by more than just a few decibels, the thickness needed to fulfill the requirements would be unworkable. In fact, even if we neglect the indirect transmissions, we would need a concrete slab of around 40 cm to meet the Spanish Building Regulation [DB-HR, 2007].
Thus, a more efficient way to improve the impact sound insulation is to put some coverings to reduce the energy that reaches at the ground floor. There are two different kind of solutions used as floor coverings: the resilient floor coverings and the floating floors.
In this chapter we review the analytical expressions available to predict the improvement of impact sound insulation due to floor coverings. Then we include these coverings in our simulation by modifying the impact force spectra (in the case of resilient floor coverings) or by creating a new model (in the case of floating floors). Finally, we compare the experimental data with the results obtained.

4.1 Resilient floor coverings

When we place resilient materials like carpets, linoleums, PVC, cork, etc...between the base floor and the impact machine, we reduce the hammer force that reaches the floor. This will create a mass-spring system where the spring constant is determined by the dynamic stiffness of the flooring ($k_d = \frac{E}{h}$), the area of impact of the hammer S_h and its mass M_h. The resonance frequency of the system is [Holger, 2009]

$$f_{s0} = \frac{1}{2\pi}\sqrt{\frac{S_h E}{M_h h}}.$$

If we use the lumped element model to compute the force spectra from the ISO tapping machine (see section 1.2.1), we can take into account the influence of the resilient material only by replacing the contact stiffness of the plate with the contact

stiffness of the resilient material. That is because a resilient floor covering usually has negligible effect on the total loss factor and the bending stiffness on a heavyweight base floor [Hopkins, 2007]. Then, the improvement in impact sound insulation will be given by

$$\Delta L = 20 \log \left(\frac{|F_n|_{without}}{|F_n|_{with}} \right). \tag{4.1}$$

In the table 4.1 we show the estimated values used for the Young Modulus of some floor coverings. In figure 4.1 we can see different cases where the experimental results are compared with the values obtained from this theoretical expression. Despite the simplicity of the approximation, we can see that the results are accurate enough. The main problem is the lack of detailed experimental data of the properties of the resilient floor coverings.
Although this section is not directly related to the SEA method, these expressions allows us to take into account the influence of the resilient floor covering by changing the input force in our SEA model following the model presented in [Brunskog and Hammer, 2003].

Material	Young Modulus (MPa)
PVC	12[1]
Cork	10[2]
Carpet	3.4[2]
Polyamide	3000[3]

Table 4.1: Young Modulus values for some resilient floor coverings. [1] Obtained from page 183 in [Wilkes et al., 2005]. [2] Obtained from pages 318 and 319 in [Vigran, 2008]. [3] Obtained from the material database *CES Edupack Software*

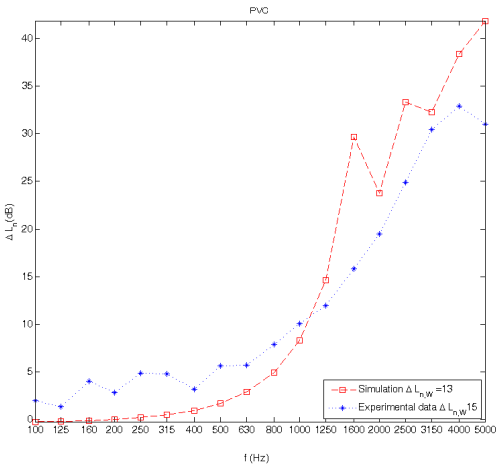

(a) 1.5 mm of PVC floor covering

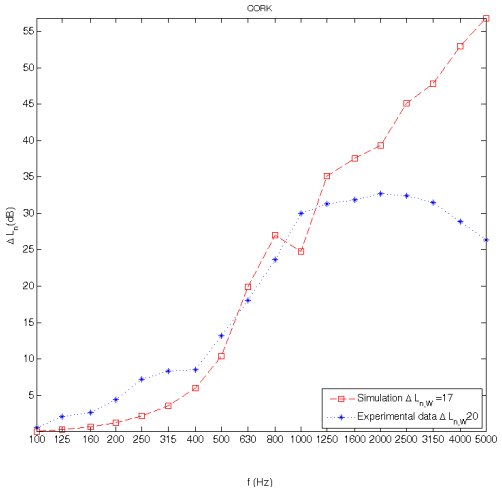

(b) 6 mm of corkboard floor covering

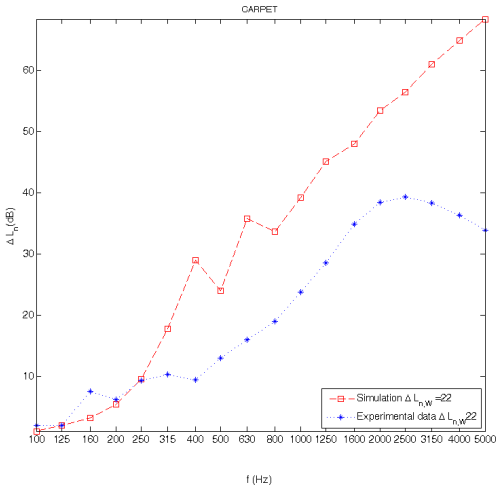

(c) 3.5 mm of carpet floor covering

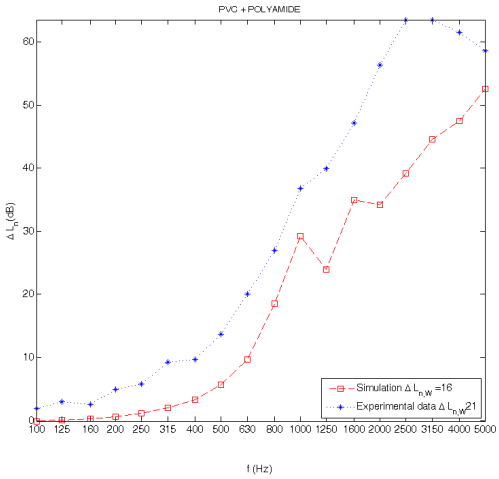

(d) 2 mm of polyamide + 2.3 mm of PVC floor covering

Figure 4.1: Improvement of impact sound insulation due to resilient floor coverings. Experimental data for figures a, b and c is obtained from reference [Buratti and Moretti, 2006]. Experimental data for figure d is obtained from reference [CSTB, 2008]. The total stiffness for figure d is obtained using $\frac{1}{k_t} = \sum_i \frac{1}{k_i}$

4.2 Floating floors

4.2.1 Introduction

A floating floor consists of a rigid surface *floating* in an elastic material above a ground floor without rigid connections between both plates. Unlike resilient floor coverings, floating floors have a complex influence in impact sound insulation. Even focusing only on heavyweight base floors, we find different kinds of floating floors depending on whether the resilient material is continuous over the entire surface, along lines or at individual points. In this section we only study the influence of floating floors with continuous resilient material. Depending on the kind of surface where the ISO tapping machine hammer impacts, we can classify these kinds of floors in [Vigran, 2008]:

- Heavyweight upper plate (typically concrete)
- Lightweight upper plate (parquet, chipboard..)

In order to develop theoretical formulations, there is a useful classification concerned with the way that acoustic waves propagate in the upper plate of the floor. Thus, we can distinguish between *resonantly reacting floors* and *locally reacting floors*. The former means floors where a reverberating bending wave is generated and, in the latter, only a limited part of the construction is supposed to transmit the force from the tapping machine. Although this classification does not have a direct equivalence with the ones presented before, a concrete slab is expected to have a reverberating behaviour because it has low internal losses, and a lightweight plate is considered to have a locally reacting behaviour due to its internal damping that forces the bending wave to extinguish before it reaches the boundaries of the plate [Vigran, 2008].

4.2.2 A concrete slab above a continuous elastic layer

This kind of solution is very common in buildings to improve impact sound insulation. As mentioned before, a resonantly reacting floor has to be assumed in order to find a theoretical approximation. In this case, we have two frequencies of interest (a detailed formulation is given in [Holger, 2009]). On the one hand, we have the frequency at which standing waves begin to appear in the elastic medium.

$$f_d = \frac{c_e}{2\pi h} \tag{4.2}$$

On the other hand, there is the resonance frequency for the mass-spring-mass

$$f_{f0} = \frac{1}{2\pi}\sqrt{k_d\left(\frac{1}{m_1}+\frac{1}{m_2}\right)}. \tag{4.3}$$

Subindex e refers to the elastic material and subindexs *1* and *2* to the upper layer and base floor respectively. k_d is the dynamic stiffness per unit area of the elastic layer. The impact sound reduction due to the floating floor (ΔL) starts at frequencies

Simulation Id Reference	Material	Thickness (mm)	Density (kg/m^3)	Young Modulus (MPa)	Loss Factor	Thickness of the slab (mm)
a [CSTB, 2003]	Polyethylene	10	61.5	0.13	0.1	40
b [LGAI, 2007]	Polyurethane	20	150	0.34	0.2	70
c [Geebelen et al., 2007]	Rock wool	40	140	0.54	0.08	50

Table 4.2: Simulation properties

over the resonance frequency with 40 dB/decade and, when standing waves begin to appear in the elastic material, the reduction changes to 20 dB/decade:

$$\Delta L = 40 \log \frac{f}{f_{f0}} \qquad (f_{f0} < f \leq f_d) \tag{4.4}$$

$$\Delta L = 40 \log \frac{f_d}{f_{f0}} + 20 \log \frac{f}{f_d} \qquad (f > f_d) \tag{4.5}$$

Different floating floors obtained from the literature have been simulated with SEA. The material properties of the floors are listed in table 4.2

To simulate the behavior of the floating floor with the commercial software VA-One, we have created two models, with and without the floating floor. Then , a tapping machine force spectra for a typical concrete floor has been introduced in both models and the resulting impact sound pressure level has been obtained. The improvement of the impact insulation given by the floating floor will be the difference between both spectra.

A problem that we find when modeling with VA-One is that the input force can only be applied to a plate, not to a Noise Control Treatment (NCT). This is related to the fact that the force must be applied to a subsystem and the NCT is not considered as a subsystem (it only modifies the SEA parameters of the neighboring subsystems), so this problem affects all the simulations made with the SEA method. Therefore, if we consider the upper plate as an NCT, when we introduce the input force it is applied directly to the ground floor (see figure 4.2a) so the model does not reproduce the behavior of a floating floor. Moreover, the elastic layer cannot be treated as a cavity because it is very thin, there are very few modes and it is meaningless to consider those dense elastic layers as cavities filled with absorbing material (figure 4.2b). Thus, we think that the best solution to simulate these floating floors is considering the upper slab as a SEA plate and the elastic layer and the ground floor as an NCT (figure 4.2c). Although it might sound strange to consider 14 cm of concrete as a noise treatment, the fact is that the results obtained are accurate enough in comparison with the experimental values.

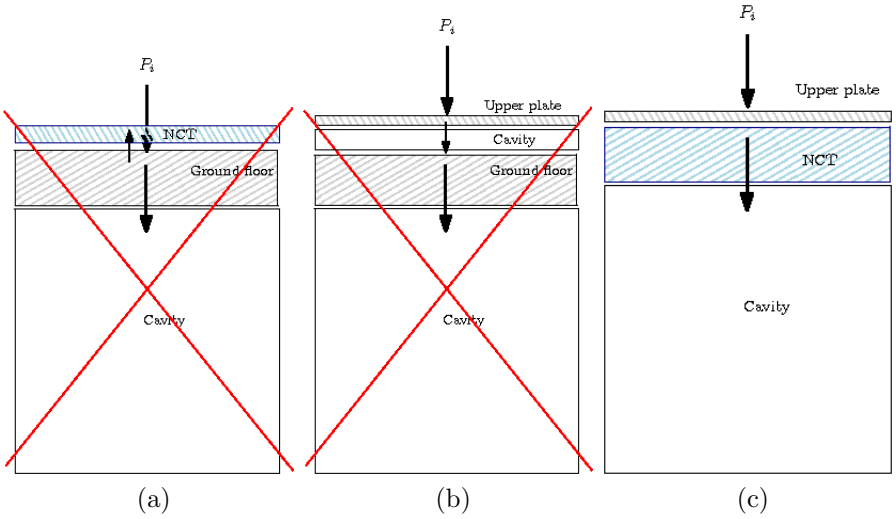

Figure 4.2: Floating floors configurations for the simulation in SEA

In figure 4.3 we see that the theoretical formulation predicts higher insulation for the floating floors than the real ones. On the other hand, in these cases, the SEA method gives 1-2 dB lower predictions. Both the experimental data and the properties of the materials are obtained from references of table 4.2 excluding the damping loss factors and the lateral dimensions, which have been estimated. In all the simulations the receiving room is a cube with 8 meter sides and the floor is a square plate placed above the cube. The lack of information has been a drawback when choosing experimental data to compare with the simulations, so there are only three cases analyzed. Although we cannot make a general evaluation of how the SEA method predicts the impact sound insulation of floating floors, we can see that the method is able to reproduce the experimental behaviour observed in these kinds of solutions.

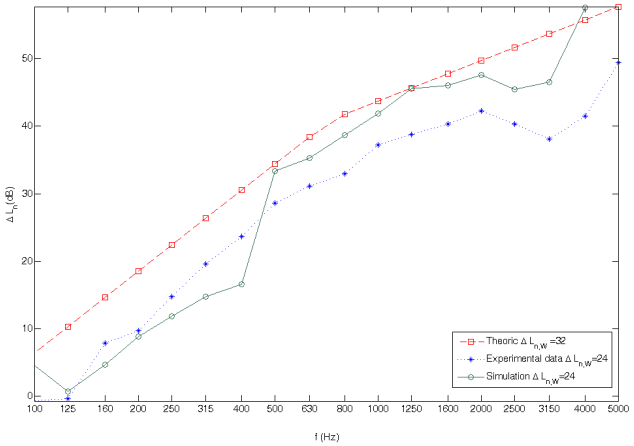

(a)

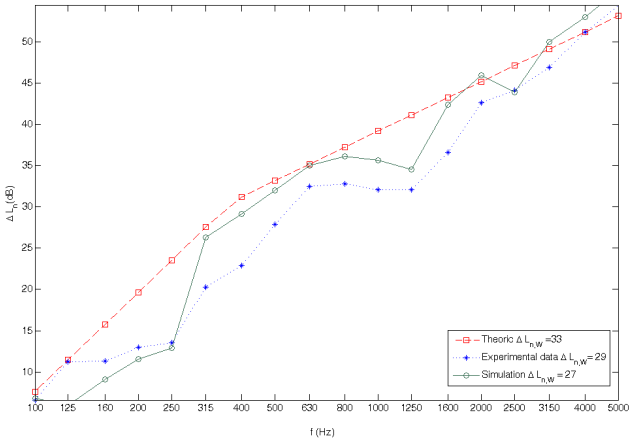

(b)

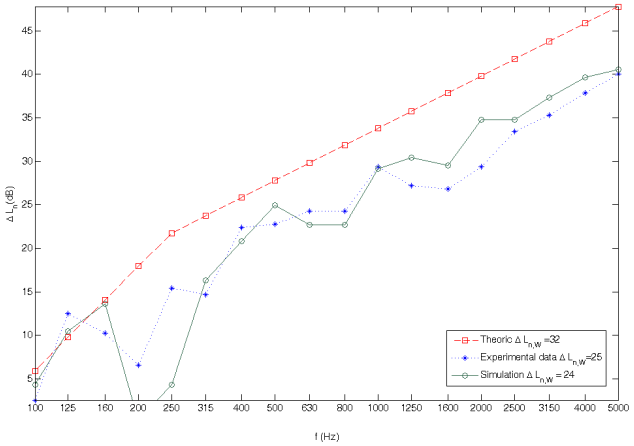

(c)

Figure 4.3: Improvement of impact sound insulation

4.2.3 A chipboard plate above a continuous elastic layer

In reference with the explanation made in 4.2.1, in this part we will try to simulate the impact sound isulation of a lightweight floating floor. Thus, in this case we have to use the theoretical formulations developed for locally reacting floors [Vigran, 2008]

$$\Delta L_n = 40 \log\left(\frac{f}{f_0}\right) + 10 \log\left[1 + \left(\frac{f}{f_z}\right)^2\right], \tag{4.6}$$

where f_z is determined by the ratio between the impedance of the floor and the impedance of the hammer

$$f_z = \frac{4\sqrt{m_s B_p}}{\pi m_h}, \tag{4.7}$$

and B_p is the bending stiffness of the floor.
In order to simulate it with SEA, the effect of the impedance in the tapping machine force will be very important. As in the previous section, the knowledge of the properties of the floor is crucial for this simulation. In this case, two different floors are simulated, whose properties are listed in the table 4.3

Material	Thickness (mm)	Density (kg/m^3)	Young Modulus (MPa)	Loss Factor
Reconstituted foam	45	100	0.18	0.015
Rockwool foam	50	160	0.38	0.015
Chipboard	22	750	3000	0.015

Table 4.3: Simulation properties

Looking at the graphs in figure 4.4, we see that SEA predictions are accurate. However, in graph 4.4b predicted values fail in the lower range and then, the global impact sound reduction obtained is very high in comparison with the experimental one. The material properties are obtained from references [Hopkins, 2007] and [Holger, 2009], excluding all the DLFs, the density of the chipboard and the Young Modulus of the chipboard, that have been estimated.

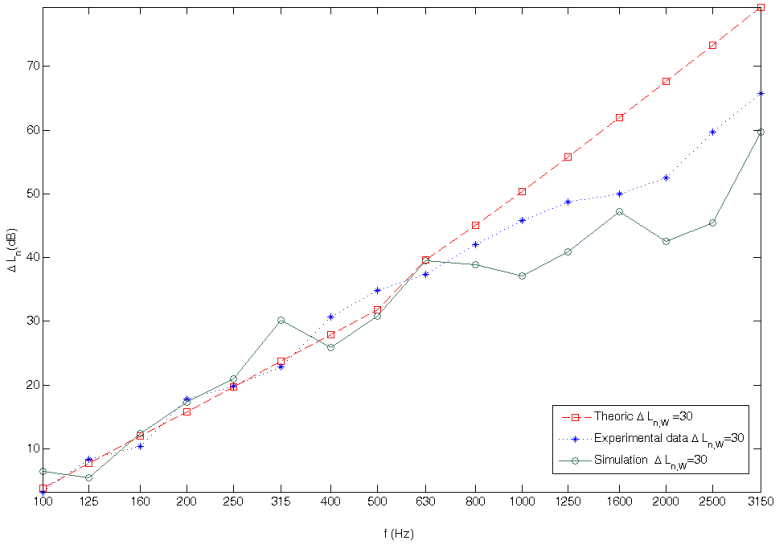

(a) Chipboard + reconstituted foam over a 14 cm concrete base floor
Experimental data obtained from p.521, [Hopkins, 2007]

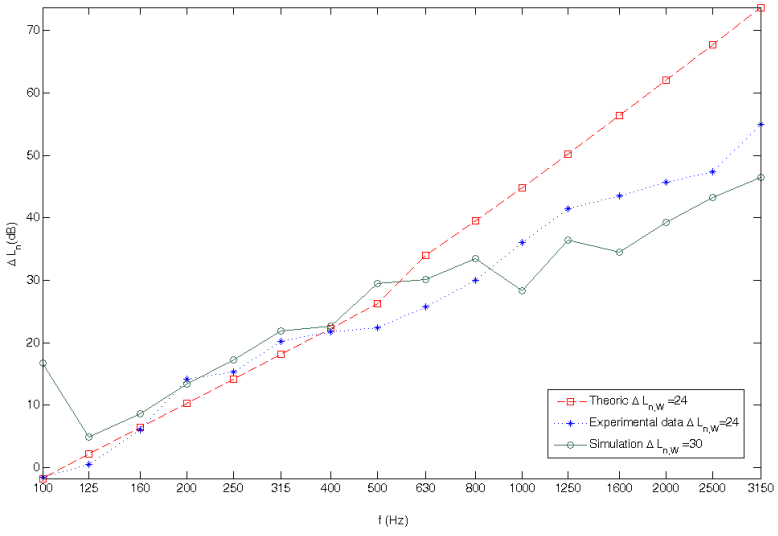

(b) Chipboard + rockwool foam over a 14 cm concrete base floor
Experimental data obtained from p.103,[Holger, 2009]

Figure 4.4: Improvement of impact sound insulation

Chapter 5

Analysis of the impact sound transmission through multiple plates

5.1 Introduction

Up to now we have studied the ability of the SEA method to predict the impact sound insulation due to the direct path. In the next two chapters we want to extend the analysis and include the influence of the structural transmission through the flanking elements. As it has been explained in section 1.1, the new regulation considers the whole building as a product, so the transmission of the impact sound due to the different elements connected to the floor also has to be taken into account.
In chapter 6 we will study the influence of the flanking transmission through the walls of the receiving cavity using the ISO model proposed in [ISO, b].
While, in this chapter we want to analyze the transmission of impact sound to other cavities not placed below the tapping machine. To perform this analysis, we consider several cases that involve the transmission through structural elements with elastic junctions. The study is focused on the influence of the rotational stiffness of the elastic material placed in the line junctions between plates. In all the cases, the different plates modeled have the same properties as in section 3.3 to compare the results with the values obtained in [Díaz, 2009].

5.2 Coupling loss factors for structural transmission

To obtain the coupling loss factor for the transmission between two plates we assume that we have a diffuse sound field in both plates. Then, the number of times per second that the energy will impact on a boundary is [Craik, 1996]

$$E_b = \frac{c_g}{\xi}, \tag{5.1}$$

where c_g is the group velocity (twice the phase velocity for bending waves) and ξ is the mean free path (the average distance that a wave has to travel between two boundaries). The mean free path for a plate with perimeter U and surface S is [Cremer et al., 2005]

$$\xi = \frac{\pi S}{U}. \tag{5.2}$$

If we want to know the energy lost in a segment $L_{p1,p2}$ of the boundary, we only have to multiply the energy by the ratio $L_{p1,p2}/U$. Then, using (5.1) and (3.3) we obtain

$$\eta_{p1,p2} = \frac{c_g L_{p1,p2} \tau_{p1,p2}}{2\pi^2 f S_{p1}}. \tag{5.3}$$

If we have an incident bending wave in an homogeneous thin plate, we can simplify this equation to [Craik, 1996]

$$\eta_{p1,p2} = \frac{c L_{p1,p2} \tau_{p1,p2}}{\pi^2 S_{p1} \sqrt{f f_{c1}}}. \tag{5.4}$$

In this case, $L_{p1,p2}$ is the junction length between both plates and $\tau_{p1,p2}$ is the transmission coefficient from plate 1 to plate 2. Chapter 5 of reference [Craik, 1996] gives the detailed formulation to derive the transmission coefficients for different kinds of junctions. If we consider the simple case of a junction between two homogeneous plates in the same plane the reduction index is given by

$$R_{p1,p2} = 20 \log \frac{\chi(1+\psi)^2 + 2\psi(1+\chi^2)}{2\sqrt{\chi\psi}(1+\chi)(1+\psi)}, \tag{5.5}$$

with

$$R_{p1,p2} = 10 \log(1/\tau_{p1,p2}). \tag{5.6}$$

The parameters χ and ψ are related to the material and thickness of the plates

$$\chi^2 = \frac{f_{c2}}{f_{c1}}, \qquad \psi = \frac{m_{p2} f_{c1}}{m_{p1} f_{c2}}. \tag{5.7}$$

Equation (5.5) is valid for rigid junctions and it provides almost the same values for the coupling loss factor between two plates than the commercial software VA-One. Instead, if we introduce an elastic isolator in the junction, other analytical expressions should be used. In references [Bosmans, 2000] and [Mees and Vermeir, 1993] we find different ways to model an elastic junction between two plates although we do not know which are the assumptions made by the VA-One. In any case, we can see in figure 5.4 that the case without isolators is the case limit of having isolators with very high stiffnesses.

5.3 Two plates with line junctions

We consider a new system with four subsystems: two plates and two cavities. The ISO tapping machine is placed in the floor on the left and we are interested in the impact sound pressure level produced in the cavity on the right. Transmission between cavities is not allowed, so we focus our analysis in the line junction that joins both plates. In figure 5.1 we can see the subsystems created in VA-One.

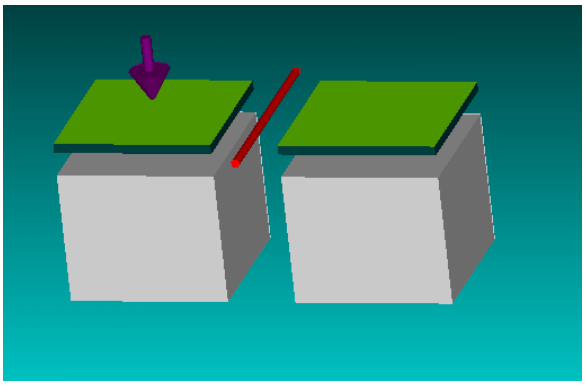

Figure 5.1: Analysis of the structural transmission between two plates

5.3.1 Modifying the rotational stiffness of the elastic joint

We now introduce a lumped spring line isolator between both plates to be able to change the stiffness of the connection between both plates. The isolator is characterized by three translational stiffnesses (K_x,K_y and K_z) and a rotational one (K_θ).

In this analysis we set all the translational stiffnesses to zero and we evaluate the effect of the rotational stiffness in the structural transmission of sound through the plates.

In figure 5.2 we see the impact sound pressure level for different values of the rotational stiffness and its comparison with the results obtained in reference [Díaz, 2009].

Observing figure 5.2b we find that, on average, the sound pressure level is 20 dB higher in the second cavity when we increase the rotational stiffness by one order of magnitude. On the other hand, in figure 5.2a we see that the sound pressure level in the first plate hardly changes.

If we compare both methods (figure 5.2b), it seems that the SEA method should give a higher value for the weighted impact sound pressure level because if we compute the mean value, it would be higher. Instead of this, due to the fact that the weighted value is more sensitive at high frequencies, the results obtained with modal methods give a weighted impact sound pressure level 4 dB higher than the SEA method.

This fact could be thought of as a problem due to the weighting process and not related to the numerical method used in the simulation. However, in figure 5.2c we see that the SEA method does not give the same values in both plates for the weighted impact sound pressure level when the rotation stiffness tends to infinity, and the modal method does.
The explanation of this anomaly lies in the foundations of SEA. When modeling a plate with deterministic methods, if we set a value for the stiffness of the junction higher than the stiffness of the plates, both plates will behave as one single plate. Whereas, increasing all the stiffness on SEA only will make the junction isolator disappear, but the system will still behave like two plates. In fact, there is no way to couple both plates in order to get the same behaviour as in a single plate - this is linked with the weak coupling between two subsystems required in SEA (see section 2.2)-. Thus, the only way to obtain the same result as with deterministic methods is considering a new model where both plates are considered as an unique subsystem (see figure 5.3).

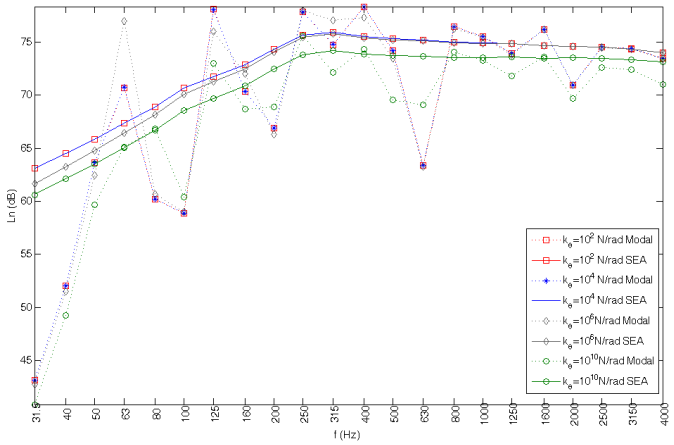

(a) First plate

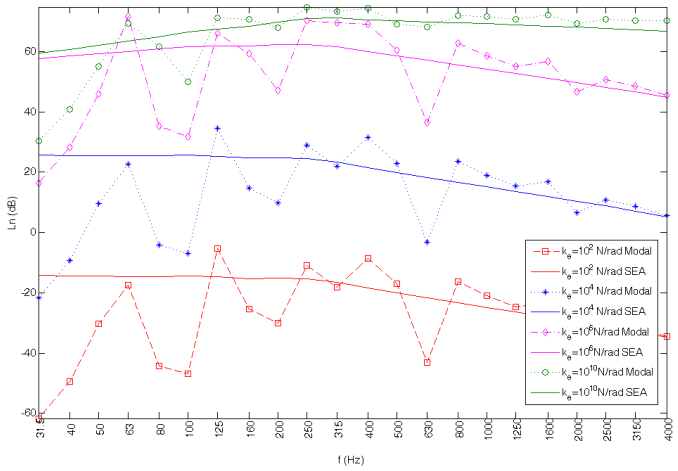

(b) Second plate

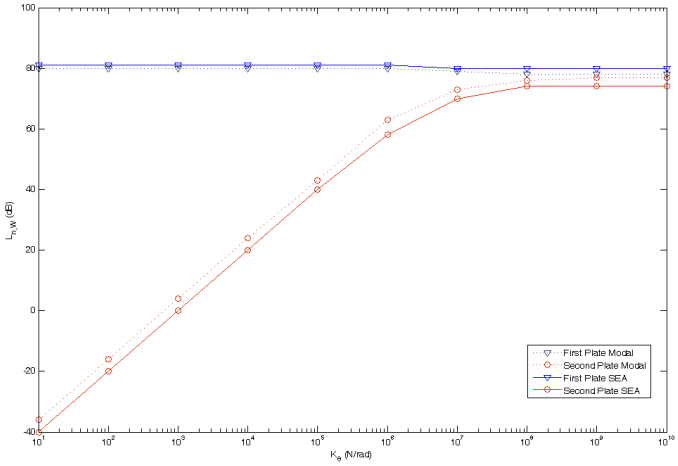

(c) Weighted normalised impact sound pressure level

Figure 5.2: Normalised impact sound pressure levels when the rotational stiffness is modified

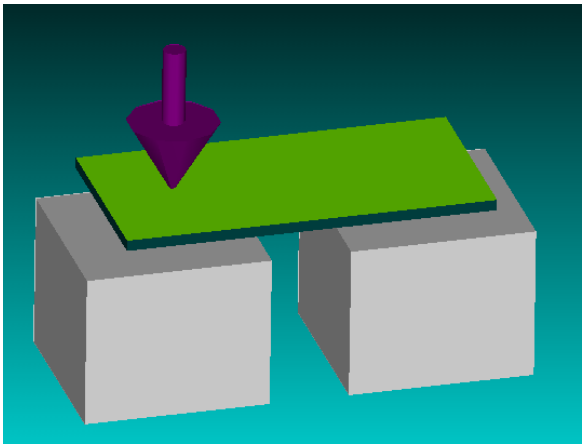

Figure 5.3: Analysis of the structural transmission between two plates

When we consider only one plate, the sound pressure level in each room is the same. That is obvious taking into account that the whole subsystem is treated as only one element in SEA, so the point of application of the input force does not matter.

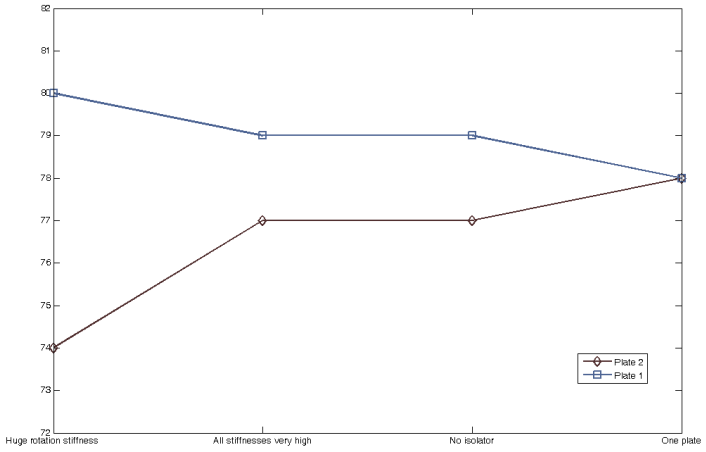

Figure 5.4: Differences in the results provided by SEA

5.3.2 Modifying the thickness of the second plate

Going on with the same model analyzed before, now we will discuss the effect of changing the thickness of the second plate in the impact sound pressure level of the receiving room. In this case, two different physical process take place in the reduction of sound transmission:

On the one hand, the change of the cross section produces an attenuation of structure-borne sound, although for thickness ratios smaller than 5, the maximum attenuation achieved is of 3 dB. A comprehensive explanation of this physical process can be found in chapter 6 of reference [Cremer et al., 2005].

On the other hand, we have seen in section 3.3 that the thickness of a plate is an important parameter for the transmission of impact sound. In all the simulations, in order to compare the results with the ones obtained in reference [Díaz, 2009], a rotational stiffness of $K_\theta = 10^8$ is used.

In figure 5.5 we see the normalised sound pressure level in the cavity on the right. Observing the graph we notice that, when the second plate is 5 cm thick, we have less sound pressure level in the low frequency range in comparison with the case when both plates are 10 cm thick. This effect is due to the difference of cross sections explained before and it is not very relevant due to the fact that the overall pressure level always diminish when the thickness of the second plate is increased.

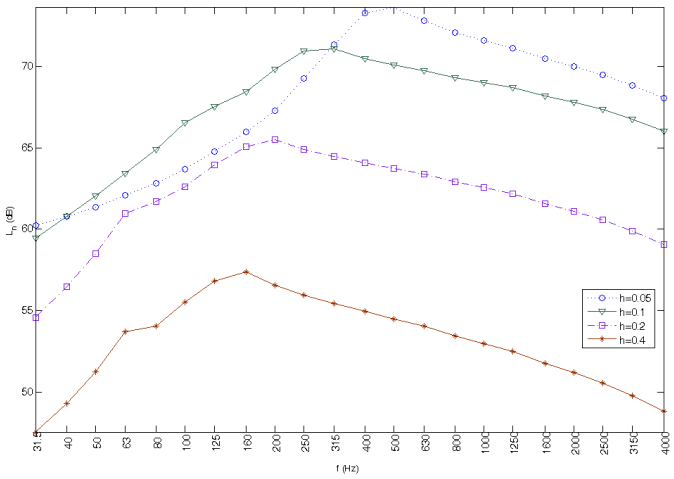

Figure 5.5: Normalised sound pressure level in the cavity below the second plate

In figure 5.6 we compare the results with the ones obtained in reference [Díaz, 2009]. We can see that, in this case, SEA results are 2 dB lower than the values using the modal approach.

Second plate thickness h(m)	$L_{n,W}$ in the first plate	$L_{n,W}$ in the second plate
0.05	80	76
0.1	80	74
0.2	80	67
0.4	81	57

Table 5.1: Weighted normalised impact sound pressure level for different thickness of the second plate

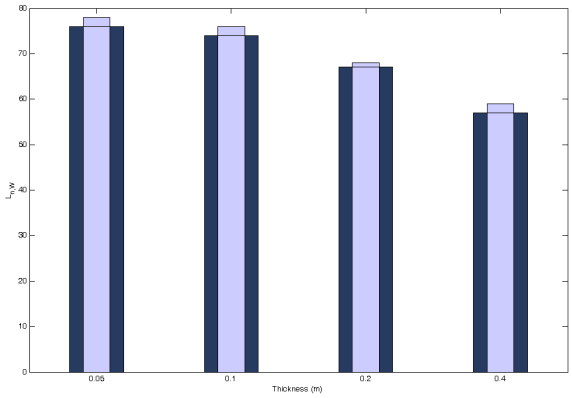

Figure 5.6: Comparison between SEA (dark blue) and the modal approach results (light blue)

5.4 Four plates with line junctions

As an extension of the section 5.3.1, we are going to analyze the influence of the rotational stiffness of the line junctions when we have four identical plates aligned. The model is displayed in figure 5.7a and the weighted normalised impact sound pressure levels for each cavity are plotted in figure 5.7b. The simulation has been done changing all the rotational stiffnesses at the same time and using the same values than in reference [Díaz, 2009]. Observing the graph, we see that the results in SEA are lower than the ones obtained with the modal approach. Besides, the difference is greater when the rotational stiffness is higher and when the cavity is further from the input force. As we can see in the figure 5.7c, the dissipation due to the internal loss factor in each subsystem is the reason to have less energy in the subsystems far away from the input source. This effect is less important when the junctions have a low rotational stiffness because most of the energy remains in the first cavity.

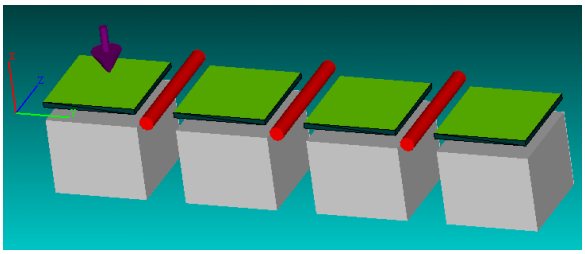

(a) Model with four plates and four cavities

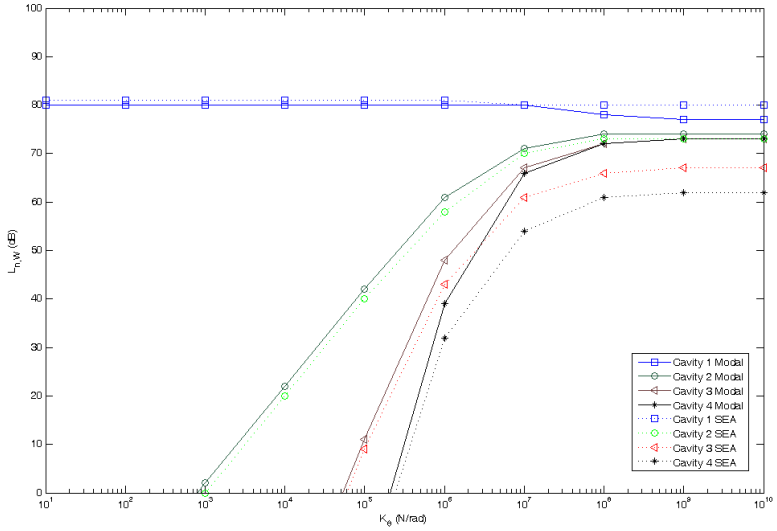

(b) Weighted normalised impact sound pressure level in the four cavities

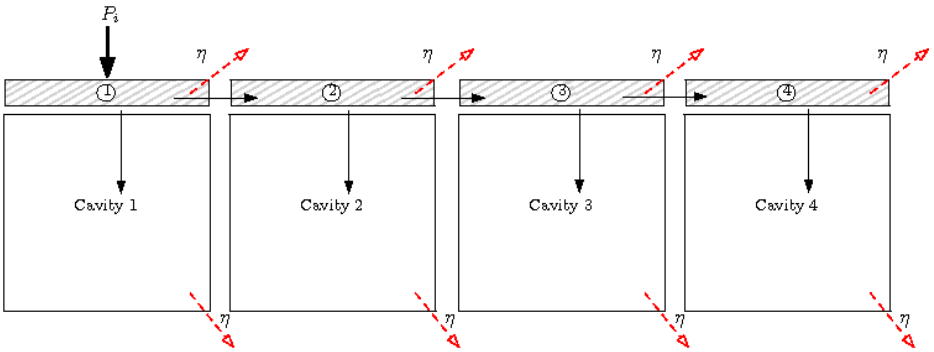

(c) Diagram of the sound transmission in SEA

Figure 5.7

5.5 T shaped structure

To finish the analysis of the performance of SEA in the transmission of impact sound trough multiple plates with elastic isolators, the T-shaped structure of figure 5.8a has been modeled. In this case, to study the influence of the rotational stiffness in the lineal junction, the transmission between cavities is not allowed. For this purpose, the coupling loss factor from each cavity to the vertical plate are set to zero (look at the diagram of figure 5.8b).

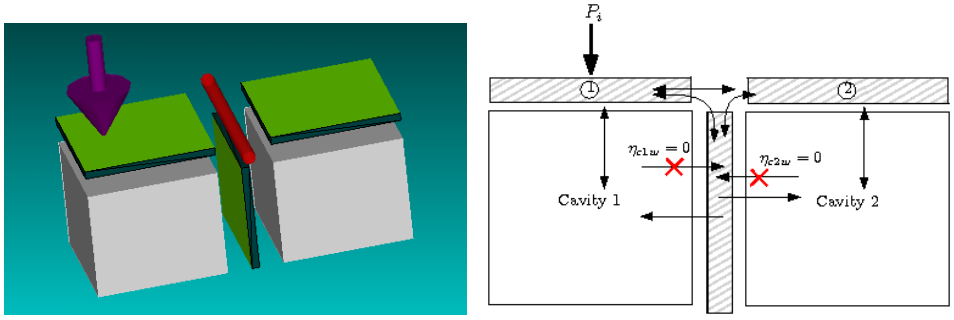

(a) T-shaped model (b) T-shaped model

Figure 5.8

The results obtained for the weighted normalised impact sound pressure levels are displayed in figure 5.9. If we compare the results with the ones obtained by modal analysis in reference [Díaz, 2009], we notice that the sound pressure level predicted by SEA in cavity 2 is 5-6 dB lower than the sound pressure level obtained by modal analysis when the rotational stiffness is lower than 10^6 N/rad but only 2 dB lower for high rotational stiffness. It seems indicate that, in this case, the influence of the junction is different in both methods.

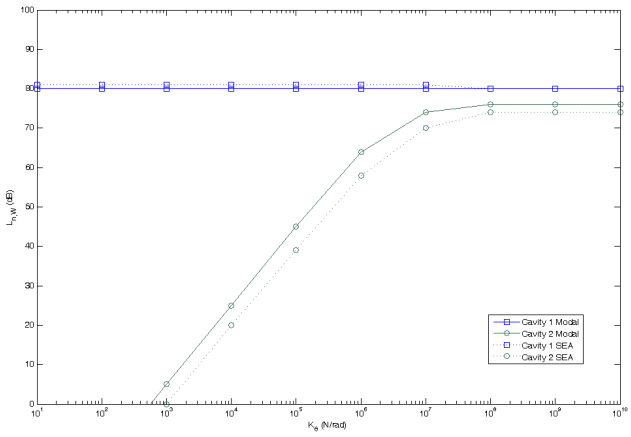

Figure 5.9: Weighted normalised impact sound pressure level in a T shaped structure

Chapter 6

Flanking transmission

6.1 Introduction

In this chapter we want to analyze the flanking transmissions through the walls surrounding the receiving room. The regulation UNE EN ISO 12354 Part-2 [ISO, b] explains the methodology that should be followed in order to calculate the flanking transmissions between two dwellings. The accuracy and limitations of this method have been analyzed in [Esteban et al., 2005] and, among the different assumptions made in the regulation we want to point out the fact that only first order flanking paths are considered. On the other hand, in [Nightingale and Bosmans, 2003] is shown that SEA gives the same expressions than the ISO 12354-1 when also only first order flanking paths are considered.

In the beginning of this chapter we present a method to decompose the SEA matrix in a group of paths. This methodology allows us to obtain the SEA expressions for the different transmission paths in a system and, specifically, for the first order flanking paths.
Besides, in order to make a comparison between the ISO expressions and SEA, we must have the same input data. Thus, we use the relationships established in [Nightingale and Bosmans, 2003] to obtain the SEA parameters from the ISO required inputs.

Finally, using the properties of the SEA method, we will analyze the influence of higher order paths in the impact sound insulation between two dwellings. In contrast with chapter 5, in this case there is no elastic material in the line junctions between plates and only simple junctions taken from [ISO, b] are considered.

6.2 Series solutions for the algebraic SEA matrix system

In this section we present the method developed by F.X.Magrans in [Magrans, 1993] to show intuitively how we can decompose a SEA matrix in group of paths. The method is also explained carefully in chapter 6 of reference [Craik, 1996].

We start the analysis writing down the general SEA power balance equations

$$\begin{bmatrix} \eta_{1T} & -\eta_{21} & \dots & -\eta_{n1} \\ -\eta_{12} & \eta_{2T} & \dots & -\eta_{n2} \\ \vdots & & \ddots & \\ -\eta_{n1} & -\eta_{n2} & \dots & -\eta_{nT} \end{bmatrix} \begin{pmatrix} E_1 \\ E_2 \\ \vdots \\ E_n \end{pmatrix} = \begin{pmatrix} \frac{P_1}{w} \\ \frac{P_2}{w} \\ \vdots \\ \frac{P_n}{w} \end{pmatrix}. \tag{6.1}$$

If we divide each row i of this matrix by its total loss factor η_{iT}, we obtain a matrix with ones in its diagonal. Then, we can decompose this matrix as a subtraction of the identity matrix I and a matrix S whose elements are defined as

$$s_{ij} = \frac{\eta_{ij}}{\eta_{jT}}. \tag{6.2}$$

Thus , we can rewrite the power balance equation in matrix notation as

$$(\mathbf{I} - \mathbf{S})\mathbf{E} = \mathbf{W}', \tag{6.3}$$

where **W'** is the power divided by $w\eta_{iT}$. To isolate the energy, we multiply both sides by $(\mathbf{I} - \mathbf{S})^{-1}$.

$$\mathbf{E} = \mathbf{W}'(\mathbf{I} - \mathbf{S})^{-1}. \tag{6.4}$$

This term $(\mathbf{I} - \mathbf{S})^{-1}$ can be expanded as series to give

$$\mathbf{E} = (\mathbf{I} + \mathbf{S} + \mathbf{S^2} + \mathbf{S^3} + \dots)\mathbf{W}'. \tag{6.5}$$

It can be seen that **the terms [i,j] in the matrix contain the group contribution of the paths from subsystem j to subsystem i**. Therefore, the matrix **S** gives the contribution of the direct path (with only one CLF), the matrix $\mathbf{S}^2$ gives the contribution of first order paths (2 CLF) and so on. Thus, writing the system of equations like in (6.5) allows us to know the exact contribution of the sound transmission through each group of paths and it provides us a tool to optimize the design of the whole system.

To understand the benefits of making this decomposition, we have created a simple example. Looking at figure 6.1 we can see some subsystems labeled: the floor (1), the receiving room (2) and two of the flanking walls (3 and 4). Analyzing the contribution of each path, we are able to calculate the sound transmission through the direct path (1→2), the transmission through first order flanking paths (1→3→2, 1→4→2) and the sound transmission through second order flanking paths (1→3→4→2).

The information obtained from this analysis could tell us which junction or element should we modify to optimize the impact sound insulation of the system. In contrast, if we only solve the SEA matrix, we would obtain the impact sound pressure level due to the contribution of all flanking paths but we would loose the knowledge of the contribution of each group of flanking paths.
In addition, if we have a system with few subsystems we can calculate the contribution of each individual path (see section 6.2.1). However, if our system has many subsystems (like in real buildings) it is very difficult to know the exact contribution of each individual path. In this context, we have done some advances by applying graph theory to transmission path problems in SEA ([Guasch et al., 2010a], [Guasch et al., 2010b]) .

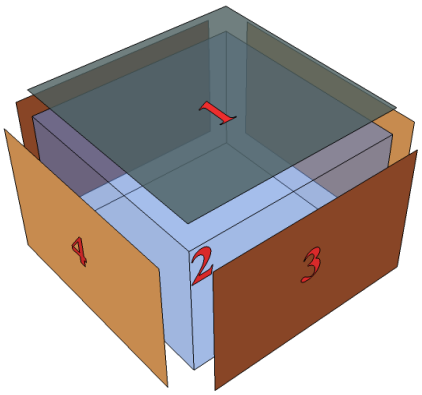

Figure 6.1

6.2.1 A 3 subsystem example

Now we consider a simple system composed of three subsystems to derive the relationships between the energy in the plate E_1 and the energy in the cavity E_2 for the different paths considered.

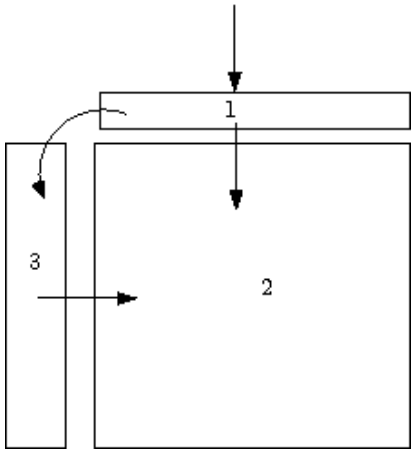

Figure 6.2: Model and paths analyzed

In this case, it is easy to see that the matrixes $\mathbf{S}$ and $\mathbf{S}^2$ are

$$\mathbf{S} = \begin{bmatrix} 0 & s_{21} & s_{31} \\ s_{12} & 0 & s_{32} \\ s_{13} & s_{23} & 0 \end{bmatrix} \qquad \mathbf{S}^2 = \begin{bmatrix} s_{21}s_{12} + s_{31}s_{13} & s_{31}s_{23} & s_{21}s_{32} \\ s_{32}s_{13} & s_{12}s_{21} + s_{23}s_{32} & s_{12}s_{31} \\ s_{23}s_{12} & s_{13}s_{21} & s_{13}s_{31} + s_{23}s_{32} \end{bmatrix} \tag{6.6}$$

As we want to know the energy transmitted from subsystem 1 to subsystem 2, we must look at the term [2,1] of each matrix. Thus, we obtain

- Direct transmission :

$$E_2 = E_1\mathbf{S}[2,1] = E_1 s_{12} = E_1\frac{\eta_{12}}{\eta_{2T}} \tag{6.7}$$

- First order flanking paths :

$$E_2 = E_1\mathbf{S}^2[2,1] = E_1 s_{13}s_{32} = E_1\frac{\eta_{13}\eta_{32}}{\eta_3\eta_2} \tag{6.8}$$

These results will be used in the next section. As a generic result, the energy from E_1 to E_n along the path 1-2-3 ... n is [Craik, 1996]

$$E_n = E_1\frac{\eta_{12}\eta_{23}\eta_{34}\ldots\eta_{n-1n}}{\eta_2\eta_3\eta_4\ldots\eta_n}. \tag{6.9}$$

6.3 Equivalence between SEA first order flanking paths and the ISO approach

6.3.1 Obtaining the SEA parameters

The first thing that we need to compare the ISO 12354-2 with the SEA method is to have the same input data in both methods. Thus, we need to establish a relationship between the SEA parameters (TLFs, CLFs and input power) and the ISO input data (Sound Reduction Index, Impact sound pressure level, surface density, geometry, etc...).

To achieve this goal, we will use the relationships derived in [Nightingale and Bosmans, 2003] for the study of airborne sound insulation, and we will apply them to the analysis of impact sound insulation. In table 6.1 we show the main parameters used by each of the methods.

In this section, subscripts i and j refer to generic subsystems, subscript *1* refers to the floor, subscript *2* refers to the receiving cavity and subscript *3* refers to a generic flanking wall.

SEA	ISO
Damping loss factor of each subsystem η_i	Normalised impact sound pressure level for the floor L_n
Coupling loss factor between all subsystems η_{ij}	Sound reduction index of all structural elements R
Power input P_i	Vibrational reduction index between all structural elements K_{ij}
	Structural reverberation time in laboratory T_{lab}
	Structural reverberation time *in situ* T_{situ}

Table 6.1: List of parameters needed

Total loss factors

In [Nightingale and Bosmans, 2003] we find a relationship between the total loss factor of a plate and the equivalent absorption length of the ISO

$$\eta_i = \frac{a_{i,situ} c}{\pi^4 S_i \sqrt{f f_{ref}}}, \tag{6.10}$$

where $f_{ref} = 1000$ Hz and $a_{i,situ}$ is given in UNE EN ISO 12354-1 [ISO, a] as

$$a_{i,situ} = \frac{2.2\pi^2 S_i}{c T_{situ}} \sqrt{\frac{f_{ref}}{f}}. \tag{6.11}$$

S_i is the area of the plate and T_{situ} is the structural reverberation time ($T_{situ} = \frac{2.2\pi}{\eta_{situ}}$).

There are several expressions to take into account the *in situ* conditions in the structural reverberation of an element, like the one that we can find in the Annex C of [ISO, a]. Instead, we will use a simplified expression proposed by Esteban et al. that is independent of the kind of building and material used [Esteban et al., 2004]

$$10 \log \eta_{situ} = -10.9 - 4.8 \log \left(\frac{f}{100} \right). \tag{6.12}$$

On the other hand,the total loss factor of the cavity can be estimated reasonably by considering only the damping loss factor of the cavity (see page 96 in [Hopkins, 2007]). Thus, it can be obtained using equation (3.16).

Coupling loss factors

The coupling loss factor between the plate and the cavity is given by the expression (3.19). Moreover, in [Nightingale and Bosmans, 2003] we find a relationship between the radiation efficiency and the *in situ* transmission coefficient

$$\sigma_{ij} = \sqrt{\frac{2\pi f^3 \eta_i \rho_i^2 \tau_{i,situ}}{\rho c^2 f_{c,i}}} \tag{6.13}$$

Otherwise, the transmission coefficient is obtained from the *in situ* sound reduction index using

$$\tau_{situ} = \frac{1}{10^{R_{situ}}}. \tag{6.14}$$

And the relationship between R_{situ} and the sound reduction index in laboratory is given by [ISO, a]

$$R_{situ} = R - 10 \log \frac{T_{situ}}{T_{lab}}. \tag{6.15}$$

T_{lab} is the structural reverberation time in laboratory ($T_{lab} = \frac{2.2\pi}{\eta_{lab}}$). In this case, the simplified formula from the UNE EN 12354-1 will be used

$$\eta_{lab} = \eta_{int} + \frac{m_p}{485\sqrt{f}}. \tag{6.16}$$

To find the coupling loss factor between two plates we use the equivalence from [Nightingale and Bosmans, 2003] between the structural transmission coefficients and the vibrational reduction index

$$10 \log \left(\sqrt{\frac{1}{\tau_{ij}\tau_{ji}}} \right) = K_{ij} + 5 \log \left(\sqrt{\frac{f_{ref}^2}{f_{c,i} f_{c,j}}} \right). \tag{6.17}$$

Using (5.4) we can obtain the expression for the coupling loss factor as a function of the vibrational reduction index. Moreover, due to the consistency relationship (3.20), we have that

$$\tau_{ij} = \sqrt{\frac{f_{c,j}}{f_{c,i}}} \tau_{ji}. \tag{6.18}$$

Then,

$$\tau_{ij} = \sqrt{\frac{1}{\sqrt{\frac{f_{c,i}}{f_{c,j}}} 10^{\frac{K_{ij}+5\log\sqrt{\frac{f_{ref}^2}{f_{c,i}f_{c,j}}}}{5}}}}. \tag{6.19}$$

The reciprocal coupling loss factors are also obtained using the consistency relationship.

With these expressions we have obtained all the SEA parameters using the inputs required by the regulation. In figure 6.3 there is a scheme of the diagram's block that should be followed in order to obtain these parameters. We still have to link the input power with the normalised impact sound pressure level of the floor and it will be done in the next section.

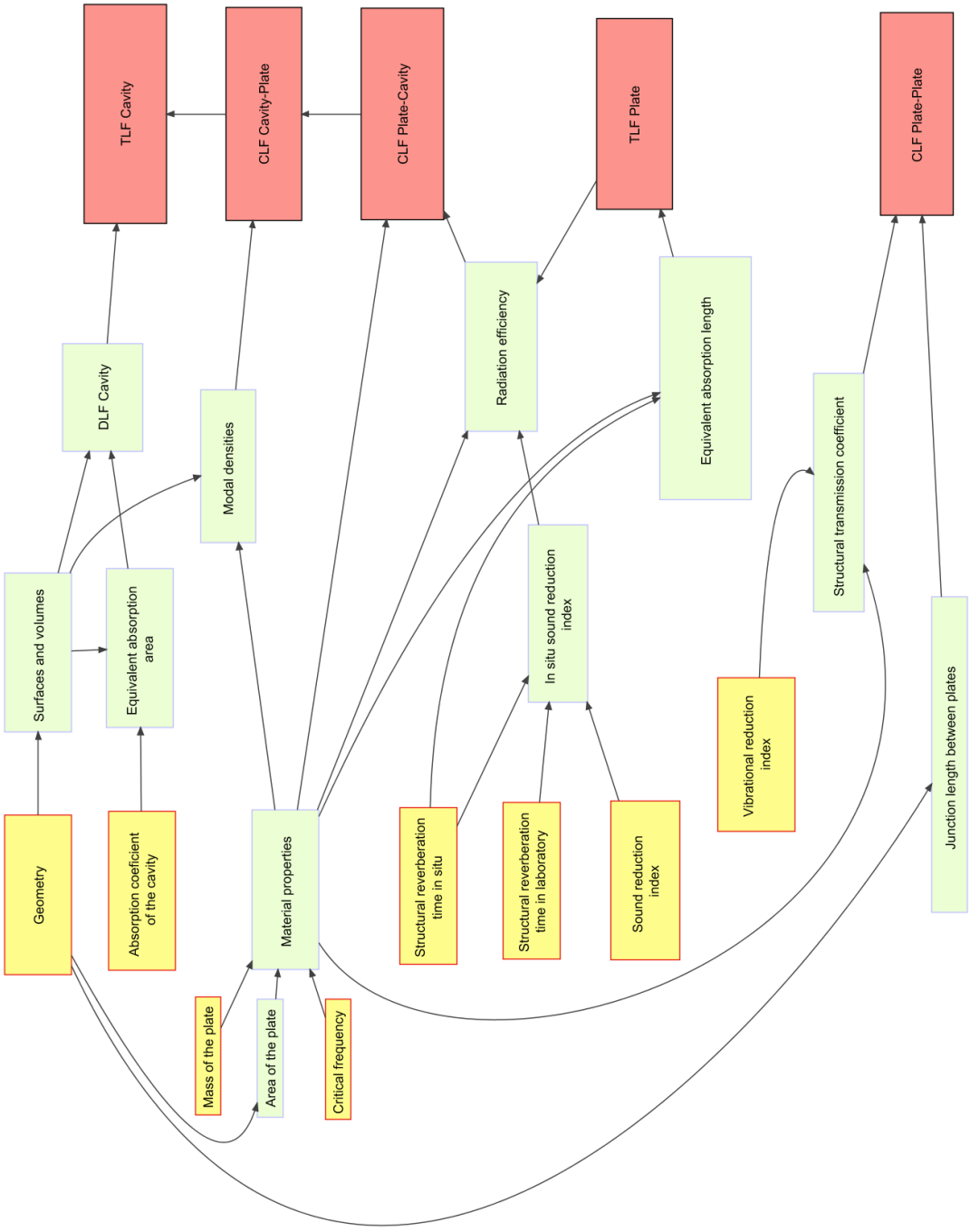

Figure 6.3: Diagram of the relationship between the SEA parameters and the input data. The ISO input parameters are displayed in yellow while the SEA parameters are plotted in red. The arrows show the way to obtain all the SEA parameters from the ISO required inputs

6.3.2 Direct path

The normalised impact sound pressure level for the direct path is given by

$$L_{n,d} = 20 \log \frac{p}{p_0} + 10 \log \frac{A}{10} = 10 \log \frac{p^2 A}{p_0^2 10}. \tag{6.20}$$

The objective of this part is to link $L_{n,d}$ with the input power of the taping machine that we introduce in the SEA power balance equations.
First of all, we start relating the pressure with the energy in the receiving cavity using:

$$E_2 = \frac{V_2 p^2}{\rho c} \tag{6.21}$$

As we are considering only the direct transmission, we can directly relate the energy in the plate with the input power (see [Craik, 1996], page 163)

$$P_1 = E_1 w \eta_{1T} \tag{6.22}$$

Then, substituting equations (6.22) and (6.7) in (6.20) we have

$$L_{n,d} = 10 \log \left(\frac{\rho c^2 A E_1 \eta_{12}}{\eta_{2T} V p_0^2 10} \right) = 10 \log \left(\frac{\rho c^2 A P_1 \eta_{12}}{V p_0^2 10 w \eta_{1T} \eta_{2T}} \right). \tag{6.23}$$

On the other hand, we can obtain $L_{n,d}$ from the laboratory measurements (L_n) using

$$L_{n,d} = L_{n,situ} = L_n + 10 \log \frac{T_{s,situ}}{T_{s,lab}}. \tag{6.24}$$

Thus, with equations (6.23) and (6.24) we have linked our input data (laboratory measurements) with the input power that we must introduce in order to be able to solve the SEA matrix.

6.3.3 First order flanking paths

Using the relationship between the energies for the first order flanking paths given in section 6.2.1, we have

$$L_{n,13} = 10\log\left(\frac{\rho c^2 A P_1 \eta_{13}\eta_{32}}{wVp_0^2 10\eta_{3T}\eta_{2T}\eta_{1T}}\right). \tag{6.25}$$

Besides, using the normalised impact sound pressure level obtained in the previous section

$$L_{n,13} = L_{n,situ} + 10\log\left(\frac{\eta_{13}\eta_{32}}{\eta_3\eta_{12}}\right). \tag{6.26}$$

Then, the remaining of this subsection is to prove that this equation is equal to the one that gives the UNE EN ISO 12354-1

$$L_{n,13} = L_{n,situ} + \frac{R_{1,situ} - R_{3,situ}}{2} - \overline{D_{v,13,situ}} - 10\log\sqrt{\frac{S_1}{S_3}}, \tag{6.27}$$

where

$$\overline{D_{v,13,situ}} = K_{13} - 10\log\frac{L_{13}}{\sqrt{a_{situ,1}a_{situ,3}}}. \tag{6.28}$$

Substituting all the parameters defined before, we obtain

$$\frac{\eta_{13}\eta_{32}}{\eta_{3T}\eta_{12}} = \frac{\cancel{\not{c}}L_{13}\cancel{\rho c}\sqrt{\cancel{2\pi f^3}\eta_{3T}\cancel{m_3^2}\tau_3}\cancel{2\pi m_1}\sqrt{\cancel{\rho^2 c^2} f c_1}\cancel{\pi^2} S_3\sqrt{\cancel{f} f_{ref}}}{\cancel{\pi^2} S_1\sqrt{\cancel{f} f c_1}\sqrt{\sqrt{\frac{fc_1}{fc_3}}10^{\frac{5\log\sqrt{\frac{f_{ref}^2}{fc_1 fc_3}}+K_{13}}{5}}}\cancel{2\pi m_3 f}\sqrt{\cancel{\rho^2 c^2} f c_3}\cancel{\rho c}\sqrt{\cancel{2\pi f^3}\eta_{1T}\cancel{m_1^2}\tau_1}a_{situ,3}\cancel{\not{c}}},$$

and, after some operations,

$$L_{n,13} = L_{n,situ} + 10\log\frac{1}{\sqrt{\tau_1}} - 10\log\frac{1}{\sqrt{\tau_3}} - K_{13} - \overbrace{10\log\left(\overbrace{\sqrt[4]{\frac{fc_1 fc_3}{f_{ref}^2}}10^{\frac{1}{2}\log\sqrt{\frac{f_{ref}^2}{fc_1 fc_3}}}}^{1}\right)}^{0} + \\ + 10\log\left(\frac{L_{13}\sqrt{\eta_{3T}}S_3}{\sqrt{\eta_{1T}}a_{situ,3}S_1}\right). \tag{6.29}$$

Substituting the total loss factors and simplifying, we have

$$L_{n,13} = L_{n,situ} + 10\log\frac{1}{\sqrt{\tau_1}} - 10\log\frac{1}{\sqrt{\tau_3}} - K_{13} + 10\log\sqrt{\frac{S_3}{S_1}} + 10\log\frac{L_{13}}{\sqrt{a_{situ,1}a_{situ,3}}}. \tag{6.30}$$

Using the expressions (6.14) and (6.28), we see that (6.30) and (6.27) are identical.

6.4 Analysis of an example

Once we have matched the SEA method with the ISO 12354-2 methodology, we are going to analyze the influence of the first order flanking paths in the impact sound insulation of a floor. Thus, we consider four flanking walls in the receiving cavity: two made of perforated bricks and two made of hollow bricks. As we have seen, in order to calculate the flanking transmissions we need the sound reduction index of all the elements. In our model, the different sound reduction indexes have been estimated using the commercial software dBKaisla[1]. The properties of the building elements used are given in table 6.2 and the model configuration is displayed in figure 6.4.

Material Flanking paths	Thickness(m)	Density (Kg/m^3)	Young Modulus (Gpa)	Loss Factor
Perforated brick 1 and 3	0.14	1500	16	0.02
Hollow brick 2 and 4	0.1	820	16	0.07

Table 6.2: Flanking elements properties

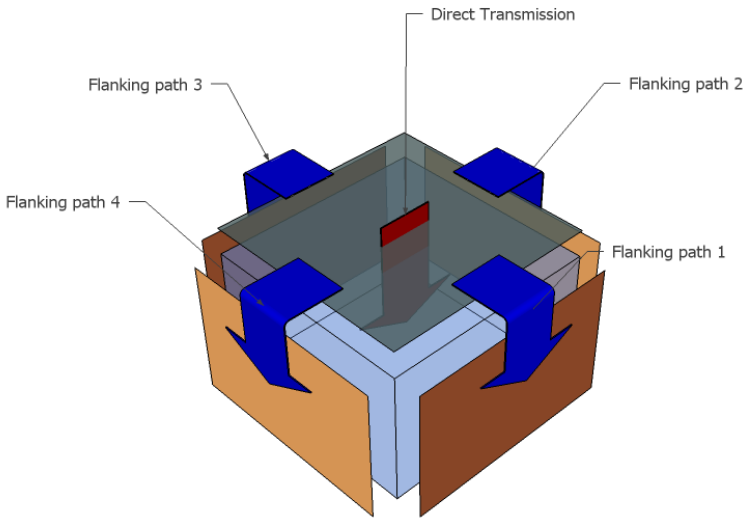

Figure 6.4: Model configuration. Direct transmission and first order flanking paths considered

In figure 6.5 we present the estimated sound reduction index for the flanking elements, as well as an estimated sound reduction index for the concrete floor considered in section 3.1.

[1] www.dbkaisla.com

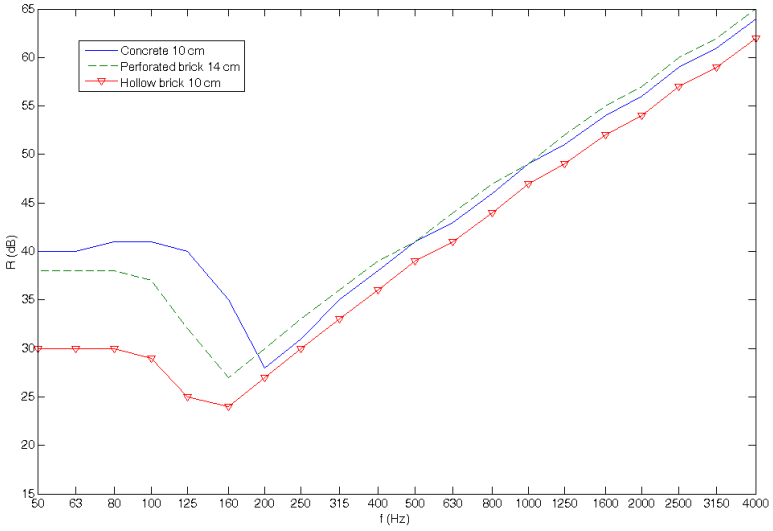

Figure 6.5: Estimated sound reduction index for different building elements

On the other hand, the structural transmission coefficient depends on the kind of junction that we consider. As we are only assuming first order flanking paths, no junction between walls is considered. The junction between the floor and the walls has been chosen as a rigid T-junction to have into account that the source room is also surrounded by walls. The vibrational reduction index is obtained from the Annex E of the UNE EN ISO 12354-1 [ISO, a]

$$K_{ij} = 5.7 + 5.7M^2, \qquad M = \log \frac{m_{p2}}{m_{p1}}. \tag{6.31}$$

Once we have calculated the direct transmission ($L_{n,d}$) and the flanking transmission for each path ($L_{n,ij}$), we can calculate the total normalised impact sound pressure level using [ISO, b]

$$L'_n = 10 \log \left(10^{L_{n,d}/10} + \sum_{j=1}^{n} 10^{L_{n,ij}/10} \right). \tag{6.32}$$

Looking at figure 6.6 we see that the normalised impact sound pressure level has been increased in ≈ 2 dB due to these flanking paths. Besides, we can see that both materials give a similar flanking sound transmission except at low frequencies, where the hollow brick has a much more lower sound reduction index and, therefore, it has a higher contribution to the total normalised impact sound pressure level.

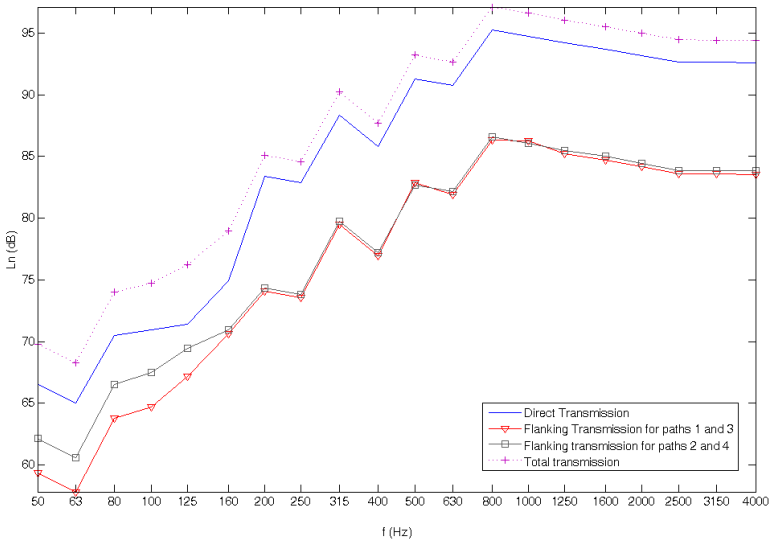

Figure 6.6: Normalised impact sound pressure level for direct transmission, flanking transmission and total transmission due to first order flanking paths for a 10 cm concrete floor

However, the contribution of the flanking transmission will be more significant as far as the impact sound pressure level due to the direct transmission becomes lower. To illustrate this behaviour, we have considered an example with a 22 cm thickness floor, made of concrete. The normalised impact sound pressure level has been predicted with the VA-One while the sound reduction index has been estimated with dBKAisla.

As we can see in figure 6.7, in this case the sound pressure level increases in ≈ 5 dB. Looking at the figure we also see that, in contrast with the previous analysis, the transmission at high frequencies is greater for the flanking paths when they are made of perforated brick walls. A possible explanation for this fact is the huge difference in the surface densities between this floor and the hollow brick walls. This difference forces a high vibrational reduction index and then, the impact sound pressure for this path is lower (see section 5.3.2). Therefore, it is important to remark that the structural transmission between elements recalls especially in the relationship between those elements.

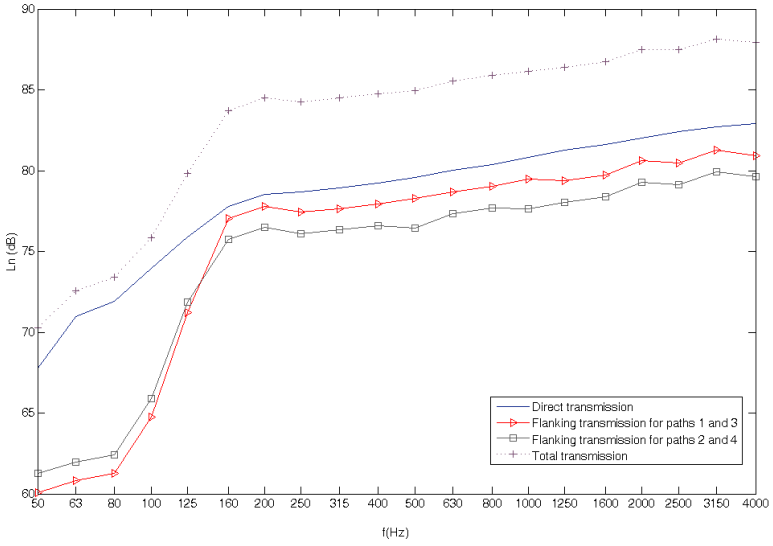

Figure 6.7: Normalised impact sound pressure level for direct transmission, flanking transmission and total transmission due to first order flanking paths for a 22 cm concrete floor

6.5 Improving the ISO prediction

In the previous section we have seen that when we take into account the flanking transmissions, the impact sound pressure level can change considerably. Moreover, in real constructions there are infinite flanking paths, so we have to expect a higher output level. In this section, we will use the same configuration than that in figure 6.6 and we will include the contributions of higher order flanking paths calculated with the method described in 6.2.

In the analysis we will consider two different cases: On the one hand, we model the junctions between the flanking walls as rigid T junctions (this means that the receiving room is surrounded by more rooms in one of the directions). On the other hand, we model the case without rooms around, so we have corner junctions with the following vibrational reduction index [ISO, a]

$$K_{ij} = \max(15|\mathrm{M}|, -3). \tag{6.33}$$

The results obtained are plotted in figures 6.8 and 6.9.

As we can see, depending on the kind of junction considered, the contribution of the high order flanking paths can be very important. While in the case of a rigid T-junction, ignoring the higher order flanking paths causes an overestimation of the insulation of 2-3 dB, if we have an isolated room the high order flanking paths have a contribution of 5-9 dB. This latter result shows the importance of modeling correctly the type of junctions and its attenuation.

Besides, in this analysis only 'short' flanking paths have been considered because no other rooms or walls have been introduced in the model. As it is shown in [Craik, 2001], long flanking paths have also a significant overall contribution and they can increase the sound pressure level in the receiving room by 5 dB.

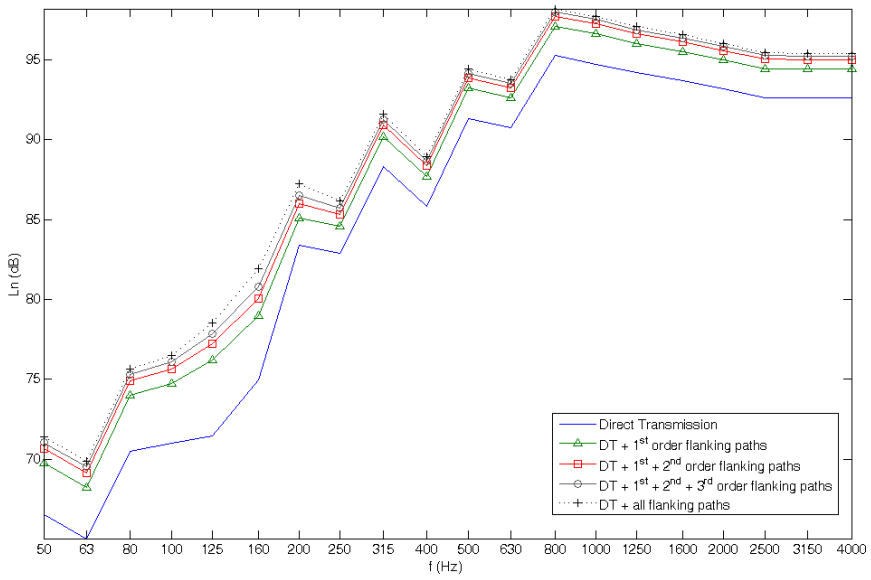

(a) Normalised impact sound pressure level for direct transmission and different order flanking paths

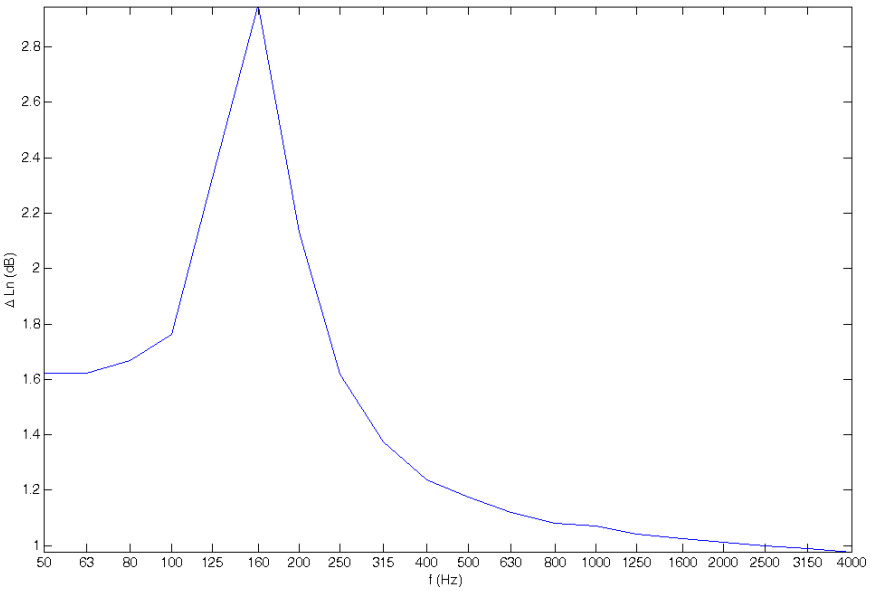

(b) Normalised impact sound pressure level difference between considering all order flanking paths and only first order flanking paths

Figure 6.8: Simulation considering rigid T junctions between flanking walls

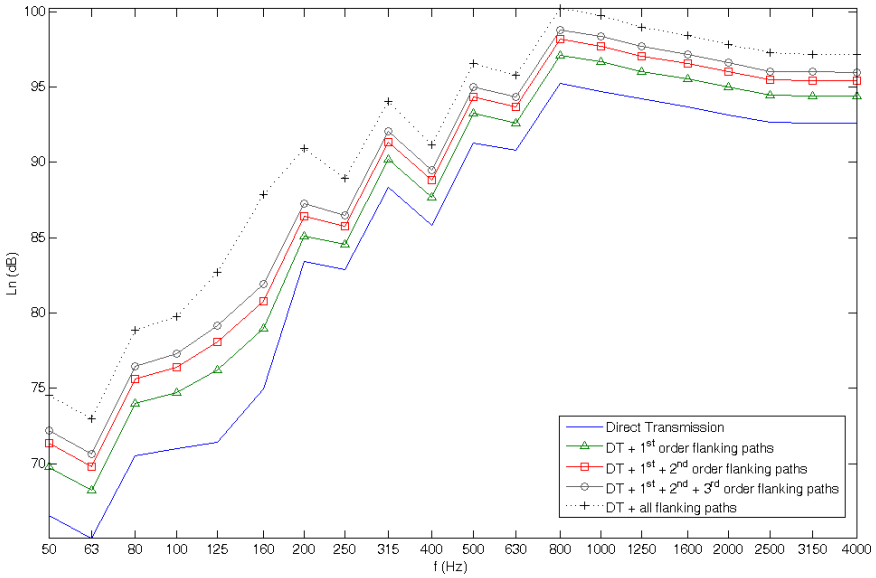

(a) Normalised impact sound pressure level for direct transmission and different order flanking paths

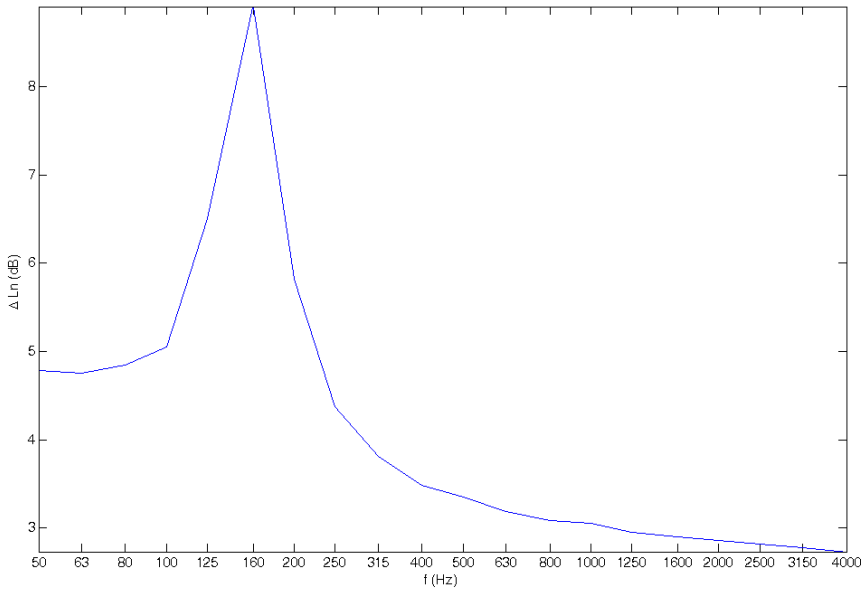

(b) Normalised impact sound pressure level difference between considering all order flanking paths and only first order flanking paths

Figure 6.9: Simulation considering corner junctions between flanking walls

Chapter 7

Conclusions and future work

Conclusions

Based on the work done we conclude that the SEA method has great advantages for its use in the prediction of impact noise. Comparison with experimental data in chapters 3 and 4 shows that the method is sufficiently reliable and can be helpful for the design of new products for impact sound insulation. In addition, chapter 5 shows the ability of SEA to predict the influence of elastic line isolators in the impact sound pressure level. In both chapters 3 and 5 we find that the results obtained using SEA agree in most cases with the values obtained by modal approaches in [Díaz, 2009].
A literature review of the theoretical expressions available for predicting the impact noise reduction of floor coverings has been made in chapter 4. In section 4.1 we have shown that the use of these analytical expressions to calculate the input power necessary in SEA can be worthwhile. In section 4.2 we have also seen that the predictions made with the software VA-One depict the behaviour of the floating floors in impact sound insulation well.
Chapter 6 shows that SEA can be very useful in calculating the sound transmission due to indirect paths. Although only a brief analysis has been made, we think that the results are very valuable showing that, in some situations, the European regulation may be overestimating the impact sound insulation of a particular building solution.
In reference to the software used, the VA-One commercial program has shown a great capacity for the simulation of the behaviour of the different elements in impact sound insulation and can be considered a good tool to make predictions. However, in some parts of this Master Thesis where an analysis of the SEA method was required, we have worked with our own code to be able to modify the input parameters.

Future work

Due to the limitation of not being able to have our own experimental data, this work has been focused on heavy floors and solutions easy to find in the literature. Even so, it would be very good to extend this analysis to lightweight floors and more complex building.

On the other hand, it would be worthwhile to go deeper into the analysis of floating floors by considering different configurations, such as connection by points or by lines.

Moreover, although this work has been related to the SEA method, a natural extension to show the capabilities of the VA-One would be the study of impact sound insulation using models that combine SEA subsystems with FEM models.

Regarding the last chapter, we think that the use of SEA to analyze flanking transmissions can improve the predictions of the European regulation. This is an open issue that has been widely addressed in the case of airborne sound insulation, but few studies have been done referring to the impact sound insulation. In addition, in reference [Guasch et al., 2010b] we show that the application of graph theory to SEA models is a valuable method to optimize the reduction of the energy transmitted from a set of sources to a set of targets. Thus, the application of graph theory to SEA impact sound transmission problems could be a promising future work.

Finally, as we have said in section 2.1, the study of the error made in SEA simulations is also necessary work to be done in the future in order to make its predictions more reliable.

Bibliography

[Arau, 1999] Arau, H. (1999). *ABC de la acústica arquitectónica*. editorial CEAC, Barcelona-España.

[Bodlund, 1985] Bodlund, K. (1985). Alternative reference curves for evaluation of the impact sound insulation between dwellings. *Journal of Sound Vibration*, 102:381–402.

[Bosmans, 2000] Bosmans, I. (2000). Analytical model for calculating structure-borne sound transmission at junctions of semi-infinite plates. *IRC Internal Report*.

[Brown, 2003] Brown, A. (2003). *The Ensemble Statistics of the Response of Structural Components with Uncertain Properties*. PhD thesis, University of Cambridge.

[Brunskog and Hammer, 2003] Brunskog, J. and Hammer, P. (2003). Prediction model for the impact sound level of lightweight floors. *Acta Acustica united with Acustica*, 89(2):309–322.

[Buratti and Moretti, 2006] Buratti, C. and Moretti, E. (2006). Impact noise reduction: laboratory and field measurements of different materials performances. Euronoise.

[Craik, 2001] Craik, R. (2001). The contribution of long flanking paths to sound transmission in buildings. *Applied Acoustics*, 62(1):29–46.

[Craik, 1996] Craik, R. J. M. (1996). *Sound transmission through buidings using statistical energy analysis*. Gower.

[Cremer et al., 2005] Cremer, L., Heckl, M., and Petersson, B. (2005). *Structure-Borne Sound.Structural vibrations and sound radiation at audio frequencies*. Springer.

[CSTB, 2003] CSTB (2003). Test report nº AC03-006/2 concerning a concrete floor. *Departement acostique et eclairage*. www.st-thermohus.dk/data/images/pdf/6.pdf, last visit on February 2010.

[CSTB, 2008] CSTB (2008). Rapport d'essais nº AC08-26015850/2 concernant un revetement de sol textile. *Departement acostique et eclairage*. www.bonarfloors.fr/document.aspx, last visit on September 2009.

[Davy, 2009] Davy, J. (2009). The forced radiation efficiency of finite size flat panels that are excited by incident sound. *The Journal of the Acoustical Society of America*, 126:694.

[Díaz, 2009] Díaz, C. (2009). Numerical modelling of impact noise. Master's thesis, Universitat Politècnica de Catalunya.

[DB-HR, 2007] DB-HR (2007). Protección frente al ruido. *Código Técnico de la Edificación*.

[ESDU, 1999] ESDU (1999). Esdu 99009:an introduction to statistical energy analysis. *Engineering Sciences Data Unit*.

[ESI-GROUP, 2009] ESI-GROUP (2009). Va-one user's guide.

[Esteban et al., 2004] Esteban, A., Cortés, A., and Arribillaga, O. (2004). In situ loss factor in Spanish hollow constructions: improving EN12354s accuracy. In *The 33rd International Congress and Exposition on Noise Control Engineering Internoise*.

[Esteban et al., 2005] Esteban, A., Fuente, M., Arribillaga, O., and López-Linares, D. (2005). Modelo de predicción de transmisión de ruido en edificios UNE-EN 12354: Precisión, limitaciones e investigaciones en el ámbito de las viviendas en españa. *Tecniacústica*.

[Fahy, 1994] Fahy, F. (1994). Statistical energy analysis: a critical overview. *Philosophical Transactions: Physical Sciences and Engineering*, 346(1681):431–447.

[Ford et al., 1974] Ford, R., Hothersall, D., and Warnock, A. (1974). The impact insulation assessment of covered concrete floors. *Journal of Sound Vibration*, 33:103.

[Geebelen et al., 2007] Geebelen, N., Boeckx, L., Vermeir, G., and Lauriks, W. (2007). Validation of a simulation program for predicting impact noise insulation of floating floors and a new method tp determine the elastic properties of resilient interlayers. *19 International Conference on Acoustics ICA*.

[Guasch et al., 2010a] Guasch, O., Aragones, A., and Janer, M. (2010a). A graph cut strategy for transmission path problems in statistical energy analysis. Submitted.

[Guasch et al., 2010b] Guasch, O., Aragonès, A., and Janer, M. (2010b). Graph cuts to reduce energy transmission in the sea model of a building. *INTERNOISE 2010, Noise and Sustainability, June 13-16, Lisbon (Portugal)*.

[Hetherington, 2009] Hetherington, J. (2009). Numerical modelling of impact noise in lightweight floors: A modal approach. Master's thesis, University of Sheffield,Universitat Politècnica de Catalunya.

[Holger, 2009] Holger, R. (2009). *Sound insulation in buildings*. Technical University of Denmark.

[Hopkins, 2007] Hopkins, C. (2007). *Sound insulation*. Butterworth-Heinemann.

[ISO, a] ISO. 12354-1: 2001: Acústica de la edificación. *Estimación de las características acústicas de las edificaciones a partir de las características de sus elementos. Parte 1: Aislamiento acústico a ruido aéreo entre recintos.*

[ISO, b] ISO. 12354-2: 2001: Acústica de la edificación. *Estimación de las características acústicas de las edificaciones a partir de las características de sus elementos. Parte 2: Aislamiento acústico a ruido de impactos entre recintos.*

[ISO, c] ISO. 140-6: 1998: Acústica. *Medicion del aislamiento acústico en edificios y de los elementos de construccion. Mediciones en laboratorio del aislamiento acústico de suelos al ruido de impactos.*

[ISO, d] ISO. 717-2: 1997: Acústica. *Evaluación del aislamiento acústico en los edificios y en los elementos de construcción. Parte 2: Aislamiento a ruido de impactos.*

[Le Bot and Cotoni, 2009] Le Bot, A. and Cotoni, V. (2009). Validity diagrams of statistical energy analysis. *Journal of Sound and Vibration.*

[Leppington and Broadbent, 2002] Leppington, F. and Broadbent, E. (2002). Acoustic radiation properties of an elastic plate with an infinite baffle and cavity. *The Quarterly Journal of Mechanics and Applied Mathematics*, 55(4):495.

[LGAI, 2007] LGAI (2007). Medición en laboratorio de la reducción del ruido de impactos transmitido a través de paneles AGLOACUSTIC de espuma de poliuretano de 20 mm sobre forjado normalizado pesado según la norma UNE-EN ISO 140-8:1998. *LGAI Technological center.* www.agloacustic.es, last visit on June 2010.

[Lindblad, 1968] Lindblad, S. (1968). *Impact sound characteristics of resilient floors coverings: a study on linear and nonlinear dissipative compliance.* PhD thesis, Division of Building Technology, Lund Institut of Technology.

[Lyon, 1975] Lyon, R. (1975). *Statistical energy analysis of dynamical systems.* MIT press Cambridge, MA.

[Magrans, 1993] Magrans, F. (1993). Definition and calculation of transmission paths within an SEA framework. *Journal of Sound and Vibration*, 165(2):277–283.

[Mees and Vermeir, 1993] Mees, P. and Vermeir, G. (1993). Structure-borne sound transmission at elastically connected plates. *Journal of sound and vibration*, 166(1):55–76.

[Nightingale and Bosmans, 2003] Nightingale, T. and Bosmans, I. (2003). Scientific Papers-Building Acoustics-Expressions for First-Order Flanking Paths in Homogeneous Isotropic and Lightly Damped Buildings. *Acta Acustica United with Acustica-Stuttgart*, 89(1):110–122.

[Price and Crocker, 1970] Price, A. and Crocker, M. (1970). Sound transmission through double panels using statistical energy analysis. *The Journal of the Acoustical Society of America*, 47:683.

[Rasmussen, 2009] Rasmussen, B. (2009). Sound insulation between dwellings-Requirements in building regulations in Europe. *Applied Acoustics*.

[Renji et al., 1998] Renji, K., Nair, P., and Narayanan, S. (1998). On acoustic radiation resistance of plates. *Journal of Sound and Vibration*, 212(4):583–598.

[R.S Langley, 2004] R.S Langley, v. (2004). Response variance prediction in the statistical energy analysis of built-up systems. *Journal of the Acoustical Society of America*.

[Sewell, 1970] Sewell, E. (1970). Transmission of reverberant sound through a single-leaf partition surrounded by an infinite rigid baffle. *Journal of Sound Vibration*, 12:21–32.

[Stewart and Craik, 2000] Stewart, M. and Craik, R. (2000). Impact sound transmission through a floating floor on a concrete slab. *Applied Acoustics*, 59(4):353–372.

[Vér, 1971] Vér, I. (1971). Relation between the normalized impact sound level and sound transmission loss. *The Journal of the Acoustical Society of America*, 50:1414.

[Vigran, 2008] Vigran, T. (2008). *Building acoustics*. Taylor & Francis Group.

[Vér, 1971] Vér, I. (1971). Impact noise isolation of composite floors. *The Journal of the Acoustical Society of America*, 50:1043.

[Wilkes et al., 2005] Wilkes, C., Summers, J., Daniels, C., and Berard, M. (2005). *PVC handbook*. Hanser Gardner Pubns.